Atmos. Chem. Phys., 25, 14333–14351, 2025 https://doi.org/10.5194/acp-25-14333-2025 © Author(s) 2025. This work is distributed under the Creative Commons Attribution 4.0 License.





# Seasonality biases arise from the interplay of retrieval quality and solar zenith angle effects in passive sensor AOD products

Sarah Smith<sup>1</sup>, Yutian Wu<sup>1</sup>, Rob Levy<sup>2</sup>, and Mingfang Ting<sup>1</sup>

<sup>1</sup>Lamont-Doherty Earth Observatory, Columbia University, New York, NY, USA <sup>2</sup>NASA Goddard Space Flight Center, Greenbelt, MD, USA

**Correspondence:** Sarah Smith (ses2271@columbia.edu)

Received: 18 November 2024 – Discussion started: 13 January 2025 Revised: 19 August 2025 – Accepted: 8 September 2025 – Published: 3 November 2025

**Abstract.** Station observations of surface Arctic aerosol have long shown a pronounced seasonal cycle, with burdens characteristically peaking in the late winter/early spring. Cloud-Aerosol Lidar with Orthogonal Polarization (CALIOP) aerosol optical depth (AOD) products replicate this seasonality, but passive sensor and reanalysis data products do not. We find that the sub- and low-Arctic seasonality of gridded AOD products from six passive sensors diverges from that of CALIOP data products during the months of September-April, even when controlling for sampling biases. Using colocated CALIOP and Moderate Resolution Imaging Spectroradiometer (MODIS) (Aqua) retrievals, we find that for colocations characterized by low-quality MODIS retrievals, the bias between MODIS and CALIOP strongly depends on the solar zenith angle (SZA), with MODIS AODs showing a 132 % reduction relative to the instrument-mean over a theoretical 0-90° SZA domain. As the fraction of MODIS retrievals flagged as "low-quality" increases with higher SZAs, retrieval quality mediates the relationship between the SZA and dataset biases in gridded products. The dependency may be the result of cloud adjacency effects, and likely also affects midlatitude AOD seasonality. Though additional sources of uncertainty in high latitude retrievals remain, the observed dependency impacts passive sensor data products' representations of (sub-)Arctic aerosol burdens in boreal spring and autumn, which are important for understanding aerosol processes in a highly sensitive yet understudied region. This work also contributes to improved understanding and quantification of the effects of viewing geometry on satellite AOD retrievals, which can help constrain aerosol observations and associated forcings, globally.

## 1 Introduction

Aerosol optical depth (AOD) is a column-integrated measure of aerosol-driven light attenuation, and it is closely related to the "direct" aerosol radiative effect. As AOD can be retrieved from spaceborne observations, it is a useful metric to assess aerosol burdens over vast and remote geographical areas. In particular, AOD can be inferred from passive sensors that observe reflected solar radiation in one or more spectral bands. Many of these passive sensors observe broad swaths, allowing them to sample most of the Earth on near-daily timescales. However, deriving AOD from passive sensors is currently difficult or impossible under many conditions (e.g.

at night, under cloudy skies, or over very high surface albedos of ice and snow). As such, their picture of global aerosol burden is still incomplete, and AOD information from passive sensors is particularly limited in the high latitudes.

In contrast to passive sensors, lidar instruments provide their own light source, deriving AOD from wavelength-specific backscatter and an inferred lidar ratio. As a result, they can process retrievals at night. Lidar products also provide vertically resolved extinction coefficient ( $\sigma_{\rm ext}$ ) profiles, representing local light attenuation along the vertical column. At night, surface reflectance affects only the lowest-altitude retrievals, allowing spaceborne lidar to retrieve over high-albedo surfaces. Retrievals through optically thin clouds, and

above optically thick clouds are also possible (Winker et al., 2009). However, the narrow footprint of the lidar makes coverage much sparser, and small-scale, transient aerosol events are less commonly detected (Smith et al., 2022; Mölders and Friberg, 2023). Still, the ability to retrieve in multiple lighting conditions and over high albedo surfaces makes lidar instruments particularly valuable in the Arctic, where extended winter darkness and widespread ice cover limit passive sensor retrievals in both winter and the shoulder seasons.

The Cloud-Aerosol Lidar with Orthogonal Polarization (CALIOP) aboard the Cloud-Aerosol lidar and Infrared Pathfinder Satellite Observations (Calipso) satellite came online in June of 2006, and was retired in August of 2023. CALIOP was the first long-term spaceborne lidar specifically designed to assess atmospheric aerosols and clouds (Winker et al., 2009). The EarthCARE satellite carrying ATmospheric lidar (ATLID) was launched in May 2024, and will continue the work of CALIOP (Haas et al., 2023). CALIOP processes retrievals by identifying and classifying optically homogeneous layers from a backscatter profile as either clean air, cloud, or aerosol; in the version 4 algorithm, aerosol layers are subsequently classified as one of seven aerosol subtypes (dust, polluted dust, dusty marine, marine, polluted continental, elevated smoke, clean continental), with each subtype corresponding to an attendant lidar ratio (Winker et al., 2009; Kim et al., 2018). This lidar ratio (S) relates the observed backscatter ( $\beta$ ) to an extinction coefficient ( $\sigma_{\text{ext}}$ ):

$$S = \frac{\sigma_{\text{ext}}}{\beta} \tag{1}$$

where *S* is given in steradians [sr],  $\sigma_{\rm ext}$  in km<sup>-1</sup>, and  $\beta$  in km<sup>-1</sup> sr<sup>-1</sup>. Accordingly, accurate representation of AODs depends on selecting the correct lidar ratio, and so potential errors in aerosol subtyping are a source of uncertainty (Kim et al., 2018). Globally, CALIOP AODs are biased low relative to MODIS, a result of CALIOP's categorization of optically thin layers as clean air, when vertically integrated measures from the passive sensors detect statistically significant aerosol reflectance (Kim et al., 2017; Toth et al., 2018).

CALIOP AODs are flagged as occurring either during the night or day, with attendant, slight differences in processing algorithms (Kittaka et al., 2011). Daytime AODs show systematically lower values than nighttime AODs, a result of the lower signal-to-noise ratio (SNR) from solar irradiance during the day (Kittaka et al., 2011). Such biases make examinations of the seasonality of high latitude AODs challenging - above 60° N, daytime AODs are infrequent during winter, while nighttime AODs are absent in midsummer (Di Pierro et al., 2013). Using the version 3 CALIOP data, Di Pierro et al. (2013) find that a linear scaling factor can be used to calculate a "nighttime-equivalent" AOD value for monthly mean Arctic AODs, though differences in the high latitude subtyping schemes between versions 3 and 4 bring into question whether the relationship remains consistent between versions (Kim et al., 2018). In the L3 version 4 CALIOP data, year-

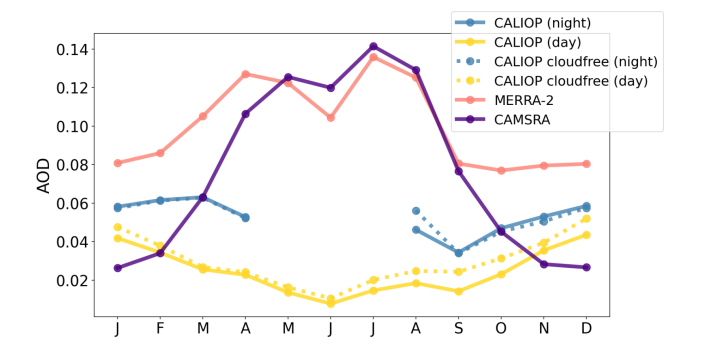


**Figure 1.** Area-weighted monthly median AOD from 65–72° N for Level 3 CALIOP day (yellow) and night (blue) datasets, for both cloudfree (dashed) and all-sky products (solid), and MERRA-2 (pink) and CAMSRA (purple) reanalysis products from January 2007–December 2021.

round monthly mean AODs are available up to 72° N, allowing for characterization of low (but not high) Arctic seasonality with just the CALIOP day data.

In situ observations of surface-level Arctic aerosol generally show a pronounced seasonal cycle, with burdens characteristically peaking in the late winter/early spring (the socalled "Arctic haze") and reaching a minimum in early to mid-summer (e.g., Mitchell et al., 1956; Rahn et al., 1977; Shaw et al., 1995). Long-term reductions in European, and more recently East Asian emissions, along with recent increases in boreal wildfire in late summer, have likely dampened the amplitude of the seasonal cycle in recent years (Quinn et al., 2007; Yang et al., 2020; Tao et al., 2020; Mc-Carty et al., 2021; Schmale et al., 2021; Smith et al., 2022). Still, Schmeisser et al. (2018) found that in four of six Arctic stations examined (2012–2014), both absorption and scattering coefficients (550 nm) peaked in the late winter/early spring and exhibited minima in summer, with the peak an order of magnitude greater than the minima in all such cases. Concentrations of sulfate (SO<sub>4</sub>) and equivalent black carbon (eBC) at the same stations showed similar seasonality when considered through 2020 (Schmale et al., 2022).

In the Arctic, where daily solar insolation varies substantially from season-to-season, constraining aerosol direct and indirect radiative effects depends on properly constraining aerosol seasonality (Quinn et al., 2008; AMAP, 2015; Zhao et al., 2015). Historically, models have largely failed to represent the seasonality of observations at monitoring stations, though in the last decade refined parameterizations of black carbon (BC) aging have improved model representations of BC seasonality, specifically (Huang et al., 2010; Eckhardt et al., 2015; Shen et al., 2017). Reanalysis AOD products assimilate observations from passive sensors with modeled transport, offering the promise of widespread coverage even where direct observations are not available. Yet, comparison of low-Arctic (65–72° N) AOD from CALIOP night and day data products, with the Modern-Era Retrospective analysis

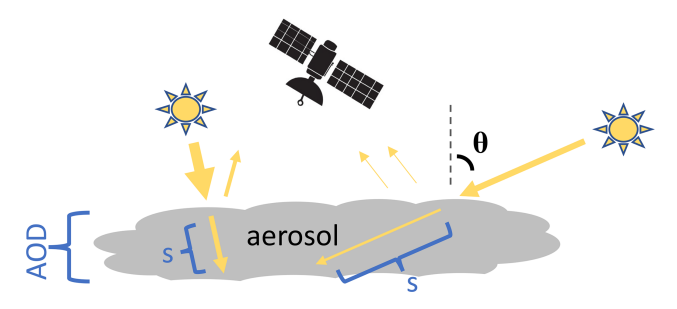


**Figure 2.** A schematic illustration of insolation and reflectance at low (left) and high (right) solar zenith angles ( $\theta$ ), where 's' shows an idealized path through the aerosol. Aerosol Optical Depth (AOD) relates to the light attenuation that would occur along a vertical path through an aerosol, and is inferred from measured reflectance (passive sensors, shown) or backscatter (active sensors).

for Research and Applications, Version 2 (MERRA-2) and Copernicus Atmosphere Monitoring Service (CAMSRA) reanalysis AODs, shows nearly opposite seasonality (Fig. 1). This is true for both the all-sky CALIOP data and the cloud-free data. Given the sensitivity of Arctic temperatures to seasonal variations in radiative forcing, understanding and constraining the seasonality of Arctic AOD is necessary for improved constraints on Arctic warming under various emissions scenarios (Bintanja and Krikken, 2016).

It is yet unclear the extent to which dataset differences in Arctic AOD seasonality are propagated from assimilated passive sensor retrievals, or are primarily the result of transport processes in models. Kittaka et al. (2011) found that biases between CALIOP version 2 and MODIS (Aqua) Collection 5 AODs show notable spatiotemporal variability, with seasonal differences in the bias particularly evident in the Southern Ocean (the authors attribute this to seasonal differences in cloudiness and wind speeds, the latter affecting ocean wave glint). Retrieval geometry has also been shown to affect passive sensor retrievals of cloud optical depth; Maddux et al. (2010) found that MODIS cloud optical depth decreased at more oblique sensor zenith angles, while Grosvenor and Wood (2014) found that MODIS liquid cloud optical depth increases with the solar zenith angle (SZA).

At high solar angles, a longer path through the atmosphere results in increased attenuation when aerosol is present (Fig. 2), as well as more diffuse scattering from neighboring clouds. Passive sensor retrievals could be affected by reduced sensitivity to higher levels of attenuation (a 1-dimensional radiative effect), or biases resulting from scattering within or between clouds and other reflective surfaces (a 3-dimensional radiative effect). Cloud contamination is a well-known source of uncertainty in aerosol remote sensing, and disentangling cloud artifacts from physical changes to cloud-adjacent aerosols remains an ongoing challenge (e.g., Remer et al., 2020). For retrievals over land, the radiative transfer module for the MODIS Dark Target product assumes a plane-parallel atmosphere, which can cause faulty

retrievals at very high SZAs (Vermote and Vermeulen, 1999). Alternatively, SZA-related differences in the CALIOP SNR could also affect the active sensor's retrieval biases, as could seasonal differences in Arctic aerosol lidar ratios if not accurately selected by the CALIOP subtyping algorithm. Of course, a combination of the above factors may also explain any observed SZA-related dependencies in the bias between CALIOP and passive sensors.

In this paper we consider three main questions in two sections. In the first section, we examine differences between CALIOP and passive sensor AOD seasonality in the sub- and low Arctic, and determine the spatial extent of differences between CALIOP and reanalysis seasonality. Second, after finding that CALIOP and passive sensors show divergent seasonality in the mid-to-high latitudes, we test the hypothesis that the bias between CALIOP and MODIS retrievals depends on the SZA. Finally, we examine the correlation between instruments as a function of the SZA, considering the utility of passive sensor data products under different SZA conditions.

#### 2 Data

For part 1 of this analysis, we consider Level 3 (L3) data from CALIOP night and day data products as well as from multiple passive sensors. L3 products are aggregated from Level 2 (L2) data, onto a regular spatial and temporal grid; L2 products are processed retrievals derived from the sensors' observations. We also compare CALIOP L3 AODs to reanalysis products from MERRA-2 and CAMSRA. For part 2 of the analysis, we compare L2 CALIOP daytime AODs from 2010 to colocated AODs from MODIS Deep Blue Dark Target combined L2 products.

# 2.1 CALIOP data

CALIOP retrieves backscatter with depolarization at 532 and 1064 nm. Subsequent processing derives aerosol subtype classifications,  $\sigma_{\rm ext}$  profiles, and AOD at 532 nm, which are available in both the L2 and L3 aerosol products. For comparisons of monthly mean gridded CALIOP versus passive sensor and reanalysis AODs, we acquired the L3 version 4.2 all-sky (CAL\_LID\_L3\_Tropospheric\_APro\_AllSky- $2^{\circ} \times 5^{\circ} \times 60 \,\mathrm{m}$ Standard-V4-20/21, and (CAL\_LID\_L3\_Tropospheric\_APro\_CloudFree-Standard-V4-20/21,  $2^{\circ} \times 5^{\circ} \times 60 \,\mathrm{m}$ ) data products. Aerosol layers over opaque clouds are, on average, optically thinner than those extending through the whole column, and as a result the AllSky CALIOP data products (which include retrievals over optically thick clouds) have a low bias relative to cloudfree CALIOP data products. The 70 m footprint of the lidar makes for less frequent sampling than passive sensors, with sampling frequencies of  $\sim 16 \, \mathrm{d}$  (Winker et al., 2009). In this analysis we consider the night and day datasets separately.

For colocations with MODIS L2 data, we acquired the CALIOP L2 profile product (CAL\_LID\_L2\_05kmAPro-Standard-V4-20/21). As the L2 CALIOP AODs were colocated with MODIS retrievals, only the daytime products were used. During level 2 processing, backscatter and depolarization ratios from each retrieval are processed using four algorithms: the Selective Iterated Boundary Locator (SIBYL), which identifies optically homogeneous layers within the profile; the cloud aerosol discrimination algorithm (CAD) which determines whether a layer is aerosol, cloud, or clear sky; the Scene Classification Algorithm (SCA) which classifies aerosol layers into aerosol subtypes; and the Hybrid Extinction Retrieval Algorithms (HERA), which uses the measured backscatter and the lidar ratios assigned to each subtype to calculate extinction within an aerosol layer (Winker et al., 2009).

Errors can occur at any level in the processing. However, classification of optically thin aerosol layers as clear sky by the CAD is a well-known source of bias, particularly for daytime CALIOP AODs; CALIOP aerosol extinction coefficients are calculated only for layers in which backscatter is detected over a noise threshold, and which are not otherwise flagged as cloud (Kim et al., 2017; Toth et al., 2018). CALIOP profile bins corresponding to layers in which backscatter falls below the noise threshold are assigned a "retrieval fill value" (RFV), and do not contribute to column integrated AODs (Toth et al., 2018). Thus, a profile in which all layers are assigned an RFV will result in an AOD of zero, even if some aerosol is present below detection thresholds (Kim et al., 2017; Toth et al., 2018). Scattering from sunlight increases background reflectance, making the noise threshold higher for daytime versus nighttime CALIOP retrievals, and resulting in systematically lower daytime AODs.

Using the version 3 CALIOP data, Toth et al. (2018) found that 71 % of all daytime profiles, and 45 % of cloudfree daytime profiles, consisted of so-called "all-RFV" profiles, in which an AOD of zero was detected. MODIS Dark Target retrievals colocated with CALIOP all-RFV profiles showed a mean value of 0.06 (0.08 for AERONET colocations), indicating that column-integrated measures detect non-negligible AOD in cases where the noise threshold for CALIOP aerosol layer detection is not surpassed.

Misidentification of aerosol subtypes, leading to incorrect lidar ratios, are additional sources of uncertainty (Kim et al., 2018). Globally, CALIOP AODs have been validated against AERONET, with a low bias (mean absolute error of  $-0.051 \pm 0.08$ ) (Kim et al., 2018). Biases at Arctic AERONET sites all fell within this range. However, because AERONET retrievals are less frequent during low-light conditions, the validation may not reflect the seasonality-related biases examined here.

#### 2.2 AVHRR data

The first in a series of Advanced Very High Resolution Radiometers (AVHRR) was launched in 1981, making AVHRR data products the longest-running satellite AOD datasets. AVHRR retrievals over ocean are processed using the Satellite Ocean Aerosol Retrieval (SOAR) algorithm (Hsu et al., 2017), and have been validated against MODIS and SeaWiFS AOD data products (Sayer et al., 2017). We use the Monthly AVHRR Aerosol Optical Thickness (650 nm) over Global Oceans version 4.0 dataset (AOT\_AVHRR\_v04r00\_monthly-avg), at 0.1° × 0.1° resolution.

## 2.3 MISR data

The Multi-angle Imaging SpectroRadiometer (MISR), which flies aboard Terra, measures reflectance from nine distinct viewing angles, allowing for improved constraints on surface reflectance and differentiation between particle types (Diner et al., 1998). We use the 555 nm optical depth from all particle types in the MISR L3 Component Global Aerosol product, version 4 (MIL3MAEN\_4), at  $0.5^{\circ} \times 0.5^{\circ}$  resolution.

#### 2.4 MODIS data

We use L2 and L3 MODIS (Aqua) AODs, from Collection 6.1 (MYD04\_L2 and MYD08\_M3 1° × 1°, respectively), with AODs at 550 nm. MODIS (Aqua) has been in use since 2002, and retrieves reflectance in 36 spectral bands (Levy et al., 2013). A viewing swath width of 2330 km allows for near-daily observations over most of the Earth (Levy et al., 2013). For both the L3 and L2 products, we use the combined Deep Blue-Dark Target (DBDT) aerosol product, which utilizes outputs from both the Deep Blue (DB) and Dark Target (DT) algorithm depending on surface characteristics and the expected retrieval accuracy for a given scene (Sayer et al., 2014). Both constituent and the merged products have been extensively validated, with DBDT AODs in MODIS Collection 6.1 showing a high bias relative to AERONET observations (mean absolute errors of 0.067, globally) (Wei et al., 2019). The radiative transfer for the DT algorithm assumes a pseudospherical atmosphere over ocean, but plane-parallel over land, while the DB algorithm uses a pseudospherical atmosphere for all retrievals.

# 2.4.1 "Negative" AODs

Since Collection 5, MODIS processing algorithms have allowed retrievals of negative AODs (values as low as -0.05) (Levy et al., 2007). MODIS optical depth retrievals depend on correct calibration of surface reflectance and aerosol properties, which can be both overestimated and underestimated. Without including negative AOD values, the dataset would selectively exclude the effects of overestimating—but not underestimating—noise in the MODIS dataset, biasing the

dataset high (Levy et al., 2007). Thus, while negative optical depths are physically meaningless, low magnitude, negative AODs in the MODIS dataset are included in the L2 retrievals, and are considered functionally similar to an AOD of zero (Levy et al., 2007).

## 2.4.2 Quality flags

Both the DB and DT algorithms operate on the same NxN boxes of native-resolution pixels, with similarities and differences in their logic and selection of appropriate wavelength band channels. Each algorithm performs similar types of data filtering, including cloud masking, snow masking, and other forms of pixel screening; however they are performed independently, defined according to algorithm-specific criteria. For DT, the remaining valid pixels are sorted so that a portion of the brightest and darkest pixels are discarded to reduce the influence of outliers; if a sufficient number of valid pixels remain, the algorithm computes a single representative top-of-atmosphere spectral reflectance vector (Levy et al., 2024). For DB, the spectral reflectance vector for each unscreened pixel is retained (Hsu et al., 2013a). Both algorithms then perform inversions by comparing these observed reflectances to values in look-up tables (LUTs), which provide expected reflectances under a range of retrieval scenarios. The AOD corresponding to the closest match between observed and LUT-based reflectances is selected as the retrieved value. Finally, while DT has already operated on a single vector to retrieve a single retrieval result in the NxN box, DB averages the multiple retrievals to provide a final result for that NxN box.

During the process for either algorithm, various indicators may arise suggesting that the retrieval may be more or less robust. These indicators are then used to assign to the retrieval a Quality Assurance and Control (QAC) flag, which conveys the algorithm's assessment of retrieval reliability. QAC values range from 0 ("no confidence") to 3 ("high confidence" or "high quality"). To receive a QAC flag of "3", several retrieval conditions must be met, depending on the algorithm and whether the retrieval occurs over land or ocean. Over ocean, high-quality MODIS retrievals require successful use of all relevant spectral channels (including 1.65 and 2.13 µm), low reflectance variability across the retrieval window, low fitting errors with LUTs, and minimal contamination from ocean glint (Hubanks, 2021). Over land, DT and DB QAC scores depend on the number of pixels remaining within a scene after masking and outlier removal; DB also accounts for the standard deviation of AOD within the scene (Hsu et al., 2013a; Hubanks, 2021). None of the QAC flag assignments depend explicitly on retrieval geometry, though retrieval geometry may influence the conditions used to assign QAC values. More detail on the thresholds used to assign each QAC score is provided in Table S1.

QAC flags of "1" or "2" are assigned when retrievals meet minimum quality thresholds but are affected by sub-

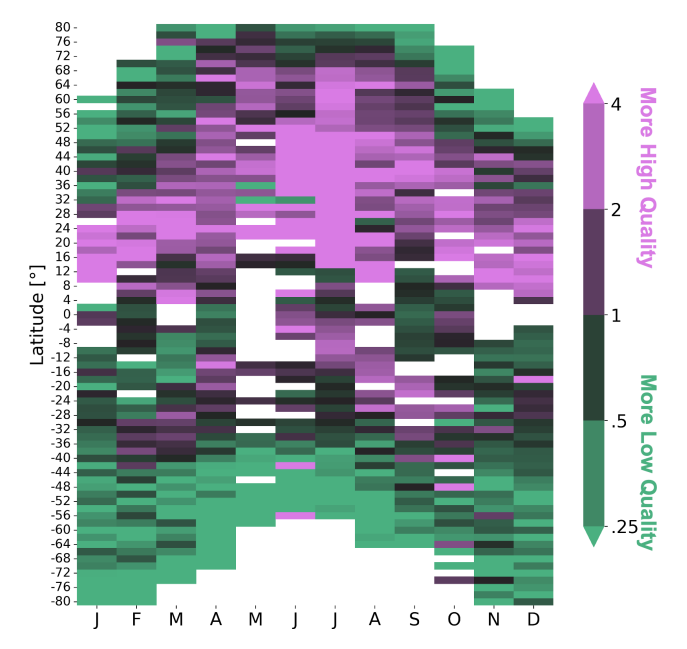


**Figure 3.** From MODIS (Aqua) L2 AODs, the ratio of 2010 MODIS QA flags of 3 (high-quality) to 1 (low-quality), binned by month and latitude. White areas indicate latitudes/months in which neither "1" nor "3" QAC flagged retrievals were available.

optimal conditions - such as a low number of valid pixels, moderate glint contamination, missing data in a shortwave infrared (SWIR) channel, elevated LUT fitting errors, or high reflectance or AOD variability. While these issues degrade retrieval confidence, they are not severe enough to warrant exclusion (QAC = 0). These lower-quality retrievals (QAC = 1 or 2) often reflect scene complexity or suboptimal viewing conditions, factors that increase the likelihood of 3-dimensional (3D) artifacts. For example, scenes containing clouds lead to a higher number of cloud-masked pixels, resulting in lower QAC scores. Cloud adjacency and other 3D effects can affect neighboring pixels by shadowing or illuminating features in ways not captured by the 1dimensional (1D) inversion. These effects represent a persistent and poorly quantified source of uncertainty in aerosol remote sensing.

The frequency of low-quality to high-quality retrievals is not uniform in space and time, with low-quality retrievals more common above 60°N from the months of October to March (Fig. 3). Similarly, retrievals over the Southern Ocean are more likely to be characterized by low QAC flags, likely the result of the glint over the area. Various L3 products utilize different averaging schemes to produce monthly mean gridded products. The DBDT product became available with Collection 6 and introduced an improved synthesis of retrievals, offering more complete spatial coverage and optimized algorithm selection. Both L2 and L3 DBDT products exclude all retrievals assigned a QAC flag of 0, while the L3 product averages the remaining retrievals without further

regards to retrieval quality. We are particularly interested in understanding biases in the L3 AOD products in areas characterized by an increased reliance on low-quality retrievals. As such, our analysis in part two is applied to valid L2 retrievals with QAC flags ranging from 1–3 (we exclude retrievals with a QAC flag of 0 from the analysis, consistent with L3 processing).

## 2.5 POLDER data

The third iteration of the Polarization and Directionality of the Earth's Reflectances (POLDER) instrument, aboard the Polarization & Anisotropy of Reflectances for Atmospheric Sciences coupled with Observations from a lidar (Parasol) Satellite, flew in the A-train from 2005-2013. POLDER collects reflectance from 12 different viewing angles across eight spectral bands, three of which provide polarized reflectances (Deschamps et al., 1994). The retrievals are processed using the Generalized Retrieval of Atmosphere and Surface Properties (GRASP) "Models" algorithm, version 2.1, with L3 products gridded to  $1 \times 1^{\circ}$  resolution (GRASP\_POLDER\_L3) (Dubovik et al., 2011, 2014, 2021). We use POLDER AODs at 565 nm in this analysis. Globally, the PARASOL/GRASP (Models) algorithm provides the greatest agreement with AERONET of the three POLD-ER/GRASP algorithms assessed in Chen et al. (2020), with R = 0.920 and 0.950 and root mean square errors (RMSEs) of 0.120 and 0.048 for 565 nm over land and ocean, respectively.

## 2.6 SeaWiFS data

We use the L3 Deep Blue AOD Angstrom Exponent product from Sea-viewing Wide Field-of-view Sensor (SeaWiFS), version 004 (SWDB L3M10,  $1 \times 1^{\circ}$ ) at 550 nm. The instrument was active from 1997-2010, and detects reflectance over eight spectral channels (Sayer et al., 2012b). The Deep Blue algorithm, which is also used in processing MODIS and VIIRS AODs, was applied to the SeaWiFS ocean and land retrievals (Sayer et al., 2012b; Hsu et al., 2013a). Validation against Maritime Aerosol Network (MAN) AODs show that 0.63 to 0.78 of SeaWiFS ocean retrievals fall within expected errors, depending on colocation selection criteria used (Sayer et al., 2012b). When validated against AERONET, land-based retrievals show considerable regional heterogeneity, with the fraction of retrievals falling within expected errors ranging from 0.46 (Southern Africa) to 0.84 (Eastern North America); however, land regions overlapping with the (sub-)Arctic region all showed acceptable performance  $(\geq 0.72 \text{ falling within expected errors})$  (Sayer et al., 2012a).

# 2.7 VIIRS data

The Visible Infrared Imaging Radiometer Suite (VI-IRS) aboard Suomi National Polar-orbiting Partnership

(Suomi NPP) is the most-recently launched instrument in this analysis, with datasets beginning in late 2011 (Wolfe et al., 2013). We use the Deep Blue L3 AOT product at 550 nm (AERDB\_M3\_VIIRS\_SNPP,  $1 \times 1^{\circ}$ , Aerosol\_Optical\_Thickness\_550\_Land\_Ocean\_Mean). Relative to MODIS, VIIRS has fewer (36 vs. 22) spectral bands, finer maximum horizontal resolution, and the AERDB product enjoys slightly improved (R = 0.848 vs. R = 0.811) correlations with AERONET, globally (Wolfe et al., 2013; Schueler et al., 2013; Li et al., 2022).

## 2.8 MERRA-2 data

The Modern-Era Retrospective Analysis for Research and Applications, version 2 MERRA-2 aerosol reanalysis product is derived from the Goddard Earth Observing System, version 5 (GEOS-5) Earth System Model, and the Goddard Chemistry, Aerosol, Radiation, and Transport (GOCART) aerosol module, which contains aerosol emissions, chemistry, and loss processes (Randles et al., 2017). AODs from MODIS, MISR, AVHRR and AERONET products are assimilated using the Goddard Aerosol Assimilation System (GAAS) (Randles et al., 2017).

Potential sources of error in the MERRA-2 product include inaccuracies in emissions estimates, model assumptions about the relationship between aerosol mass and optical properties (including aerosol hygroscopicity), and parameterization of wet deposition (Buchard et al., 2017). Validation of MERRA-2 AODs against MAN and US-based airborne high spectral resolution lidar observations showed high correlations (R = 0.93 and R = 0.85, respectively) (Randles et al., 2017). However, control simulations in which satellite retrievals were not assimilated resulted in lower correlations (R = 0.84 and R = 0.81, respectively) (Randles et al., 2017). Similarly, MERRA-2 source region extinction coefficient profiles showed greater agreement with CALIOP than the assimilation-free control run (Buchard et al., 2017). As such, it is plausible that the product may be less reliable in the Arctic, where little data is available for assimilation. Here, we use the monthly mean instantaneous single-level assimilation aerosol optical depth analysis, for AODs at 550 nm (instM\_2d\_gas\_Nx).

# 2.9 CAMSRA data

The Copernicus Atmosphere Monitoring Service reanalysis product (CAMSRA) is generated by the European Centre for Medium-Range Weather Forecasts (ECMWF), with aerosol emissions and chemistry from the Integrated Forecasting System (IFS) chemistry and aerosol module (Inness et al., 2019). The reanalysis product assimilates 550 nm AODs from MODIS Terra and Aqua, and from 2003 to 2012 the Advanced Along-Track Scanning Radiometer (AATSR) (Inness et al., 2019). Here we use the CAMSRA aerosol composition product total AOD at 550 nm.

Gueymard et al. (2020) found slightly greater RMSEs for CAMSRA versus MERRA-2 when validated against AERONET (0.126 vs. 0.144), globally; at polar sites, the RMSE was more than double for CAMSRA versus MERRA-2 (0.105 versus 0.048). As MERRA-2 assimilates AERONET, but CAMSRA does not, the extent to which reductions in RMSE reflect improved aerosol processes, rather than varying sources of assimilation, is unclear; understanding reanalysis products' capabilities and limitations away from sources of assimilation can provide better insight into the products' capabilities in the Arctic, especially in months where AERONET observations and other sources of assimilation are sparse or non-existent.

## 3 Methods

## 3.1 Comparison of gridded Arctic AOD seasonality

We obtained the above-mentioned L3 and reanalysis AOD datasets. Wavelengths of the AOD products range from 532 to 565 nm, with the exception of the 650 nm AVHRR product. Slight differences in AOD wavelength are unlikely to contribute substantially to differences in seasonality. However, in months characterized by an abundance of small particles (such as smoke), differences between AVHRR and other products may be expected. The gridded AODs were given at different horizontal resolutions. For each comparison, the coarser CALIOP AODs were regridded to the finer passive sensor and reanalysis grids, without interpolation.

## 3.2 Colocations

From June 2006 to September 2018, Calipso and Aqua flew together in the A-train, with Calipso trailing Aqua by approximately 2 min. We obtained the above-mentioned MODIS and CALIOP L2 data products for 2010, as 2010 exhibited few gaps in data availability for either instrument. Due to the high-frequency, near-simultaneous retrievals from MODIS and CALIOP, we were able to amass 138 866 strictly-defined colocations over a 1-year sampling period.

Colocations were defined as instances in which both instruments returned valid (non-NaN) AODs, and in which the midpoints of retrievals from each instrument were no more than 1 km haversine distance and occurred no more than 3 min from one another. Colocations were selected without replacement, such that a single retrieval could not appear more than once in the analysis; in cases where multiple matches were possible, the closest possible colocated pairing was selected. Prior studies have used radii of 25–50 km and temporal windows of 30–60 min when comparing satellite observations to retrievals from AERONET and DRAGON sites (e.g., Levy et al., 2013; Munchak et al., 2013; Virtanen et al., 2018). The stricter criteria made possible by the Atrain configuration makes it extremely likely that colocated retrievals are sampling the same airmass.

A similar fraction of the colocations were characterized by low ("1") and high ("3") MODIS QAC flags – 45.8 %  $(n=63\,598)$  and 52.8 %  $(n=73\,302)$ , respectively – while colocations characterized by medium ("2") MODIS QAC flags contributed just over 1 % (n=1966) to the sample. As MODIS retrieves only under low cloud-fraction conditions, colocated CALIOP AODs were therefore assumed to reflect clear or nearly-clear sky conditions. Because MODIS only retrieves during the day, all colocated CALIOP retrievals were processed using the daytime algorithm.

SZAs vary with latitude, season, and time of day. Ascending passes of the polar-orbiting A-train constellation cross the equator at approximately 13:30 local time, and SZAs for colocated retrievals therefore range from 8.58 to 80.04°. Due to the configuration of the MODIS swath, the viewing angle for colocated MODIS retrievals was near-nadir, ranging from 0.17 to 19.22°; the relatively low range for the viewing zenith angle (VZA) makes this variable well-controlled relative to the SZA. Fewer than 0.5% of the valid CALIOP day and 0.05% of valid near-nadir (< 20°) VZA MODIS retrievals were selected.

#### 4 Results

# 4.1 Arctic AOD seasonality

Above the Arctic circle, most passive sensors have limited wintertime data. However, reanalysis AODs in the Arctic may be influenced by assimilated passive sensor AODs just outside the region, so in this analysis we consider seasonality within a 60-72° N domain, from January 2007 to December 2021. Direct comparison of the seasonality of Arctic AODs from passive and lidar sensors is made challenging by the fact that there is considerable spatiotemporal variability in passive sensor data availability in the high latitudes. Figure 4 shows the spatial distribution of data availability above 60° N by instrument and season. In boreal spring (MAM), AVHRR, MISR, MODIS, and VIIRS monthly mean AODs primarily capture North Atlantic AODs, while in summer (JJA) most instruments show more uniform coverage; for MISR, MODIS, and VIIRS, autumn (SON) is characterized by a considerable latitudinal gradient in data availability, such that regionally-averaged autumnal Arctic AODs will primarily reflect sub-Arctic and low-Arctic values. As a result, characterizing Arctic AOD seasonality from the heterogeneous sampling of passive sensors is inherently challenging, and comparisons between active and passive sensors need to control for sampling biases.

To control for sampling biases, for each passive sensor we subsampled the CALIOP day datasets (both cloudfree and all-sky) to only months and gridcells where the passive sensor data were available. From each passive sensor and their corresponding subset of CALIOP AODs, we calculated areaweighted monthly mean 60–72° N AODs for each month, then found monthly medians from the 2007–2021 regionally-

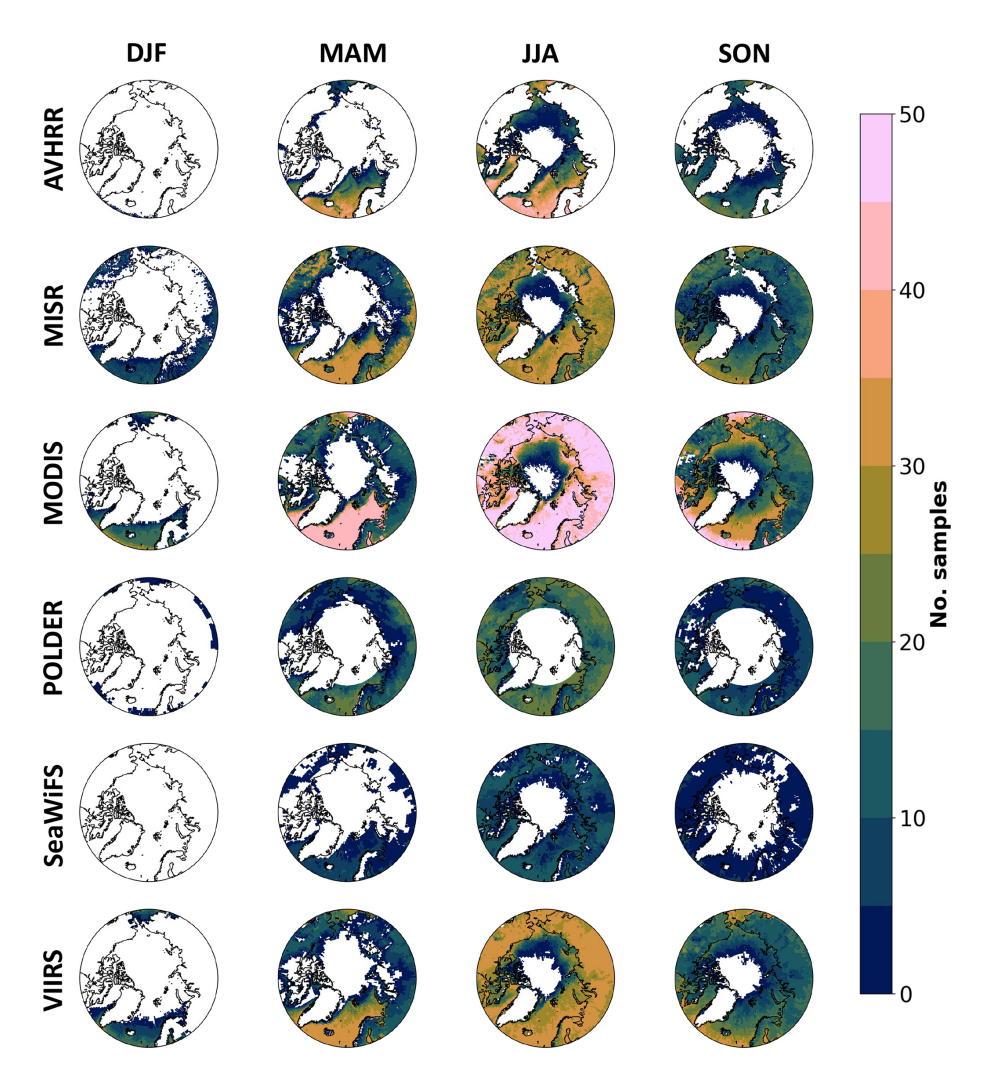


Figure 4. From 2007–2021, the number of valid L3 monthly mean samples above 60° N by season, for six passive sensor data products.

averaged AODs (Fig. 5). As this analysis is not a comparison of colocated retrievals, we also noted the number of months in the sampling period from which each monthly median value was calculated (blue numbers atop each subplot).

For MISR, MODIS, and VIIRS, the number of years with January samples is comparable to that with June samples. While AVHRR, POLDER, and SeaWiFS lack full year-round coverage, each (except AVHRR in February) has a similar number of sampled years in the low-light months as in midyear. Given the relatively stable sampling across months, wintertime median AODs are as representative of the dataset as summertime values.

In each instance, pronounced differences in seasonality between CALIOP and passive sensors were evident despite controlling for sampling biases. All passive sensors (except SeaWiFS, which has no winter AODs) show substantially lower winter versus summer AODs; for MODIS, January AODs are nearly a fourth of July values. CALIOP, in contrast, exhibits the highest AODs in winter in every subsampling, for both the all-sky and cloudfree data products.

MODIS, SeaWiFS, and VIIRS (which all make use of the Deep Blue algorithm—SeaWiFS and VIIRS exclusively) show seasonal maxima in July, with secondary peaks in April. AVHRR also shows a July peak, but with little additional seasonal structure besides an abrupt decline in AOD in February. MISR and POLDER are the only passive sensor instruments in which AOD peaks in spring rather than summer, with instruments showing maxima in April and May, respectively. Both instruments provide additional constraints on the direction of scattering through multiple viewing angles, and as a result may better control for differences between high latitude spring versus summer viewing geometries.

As passive sensors do not retrieve over clouds, the cloud-free (yellow, dashed) CALIOP data are the most apt comparison to passive sensors. In the 65–72° N comparison of CALIOP and reanalysis AOD seasonality (Fig. 1), the structure of Arctic CALIOP cloudfree AODs shows little agree-

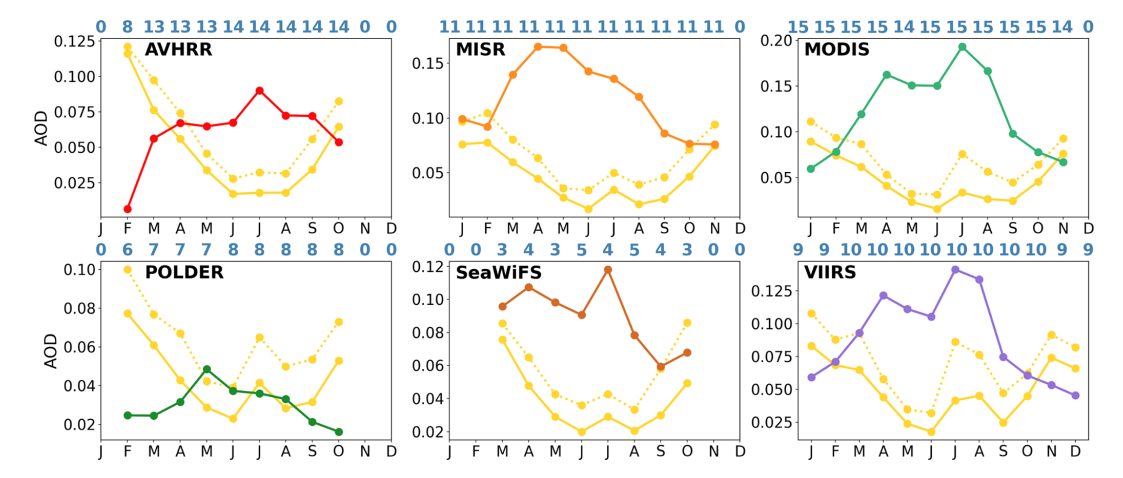


**Figure 5.** Median 60–72° N area-weighted L3 AOD from six passive sensors (assorted colors) versus CALIOP (day) all-sky (solid, yellow) and clearsky (dashed, yellow) products, subsampled to only gridcells and months in which the respective passive sensor data are available. The number of months in the sampling period (July 2007–December 2021) in which at least one gridcell was available for comparison are noted in blue above each subplot, and correspond to the monthly markers on the *x* axis below.

ment with reanalysis AODs, even during summer. In contrast, from April to September the structure of the subsampled 60– 72° N CALIOP cloudfree datasets resembles its passive sensor counterpart, particularly for MODIS, VIIRS, and SeaWiFS. Specifically, a local maximum from mid- to late summer is substantially reduced from the assessment of region-wide CALIOP monthly median AODs (Fig. 1), but is pronounced in the cloudfree datasets subsampled to MISR, MODIS, POLDER, SeaWiFS and VIIRS data availability (Fig. 5). Such differences in the structure of the CALIOP summertime Arctic AODs when sampling from the different domains suggest that sampling biases are likely to impact region-wide assessments of summertime Arctic AODs, and likely result in an overestimate of the magnitude of the late-summer peak at the regional level. However, the decoupling of the seasonal structure from early autumn through mid-spring shows that sampling biases are not sufficient to explain overall differences in seasonality.

In the midlatitudes, reanalysis AODs are constrained by passive sensor products throughout the year, so differences in reanalysis and CALIOP seasonality likely reflects differences between passive and active sensor retrievals at these latitudes. In Fig. 5, the bias between passive and active sensor seasonality was evident down to 60° N. It is yet unclear whether the bias between the seasonality of CALIOP and other gridded datasets extends beyond the high latitudes. To assess the latitudinal extent of the bias, and to separate the bias in seasonality from a bias in magnitude, for both CALIOP night and day datasets we found the monthly median zonal mean AODs, then normalized the monthly medians to their seasonal cycle. We do the same for MERRA-2 and CAMSRA AODs, then subtract the normalized reanalysis from the normalized CALIOP AODs (Fig. 6). With this

approach, we examine the bias in seasonality without regards to the magnitude of the seasonal cycle.

In each pair of reanalysis-CALIOP dataset comparisons, a bias in seasonality is evident in both hemispheres, extending from the high latitudes to approximately 40°. The bias is evident in comparisons with both the daytime and night-time CALIOP products, but is slightly more pronounced in comparisons with the daytime product.

These findings suggest that the mechanisms responsible for the bias in Arctic AOD seasonality between active and passive sensors may in fact be evident throughout much of the globe. Equally important, while CALIOP daytime AODs may be influenced by seasonal differences in insolation, CALIOP nighttime AODs are not. As such, differences in seasonality between reanalysis and CALIOP nighttime AODs are not driven by seasonal differences in the SNR, and another explanation for the difference must exist. More direct comparisons between colocated retrievals are necessary to provide further information about the mechanisms and precise magnitude of the bias.

# 4.2 A solar zenith angle dependency

We hypothesized that the bias between CALIOP and passive sensor AODs may depend on the SZA, which in turn may contribute to differences in Arctic AOD seasonality. To test this hypothesis, we compare the biases between colocated CALIOP and MODIS (Aqua) L2 AODs at different SZAs for the year of 2010.

As noted in Sect. 2.1, CALIOP returns AODs of zero when an entire profile is populated with RFVs. Toth et al. (2018) quantified the effects of all-RFV profiles on CALIOP average AODs, by comparing them to colocated MODIS retrievals. However, no studies have considered whether the frequency

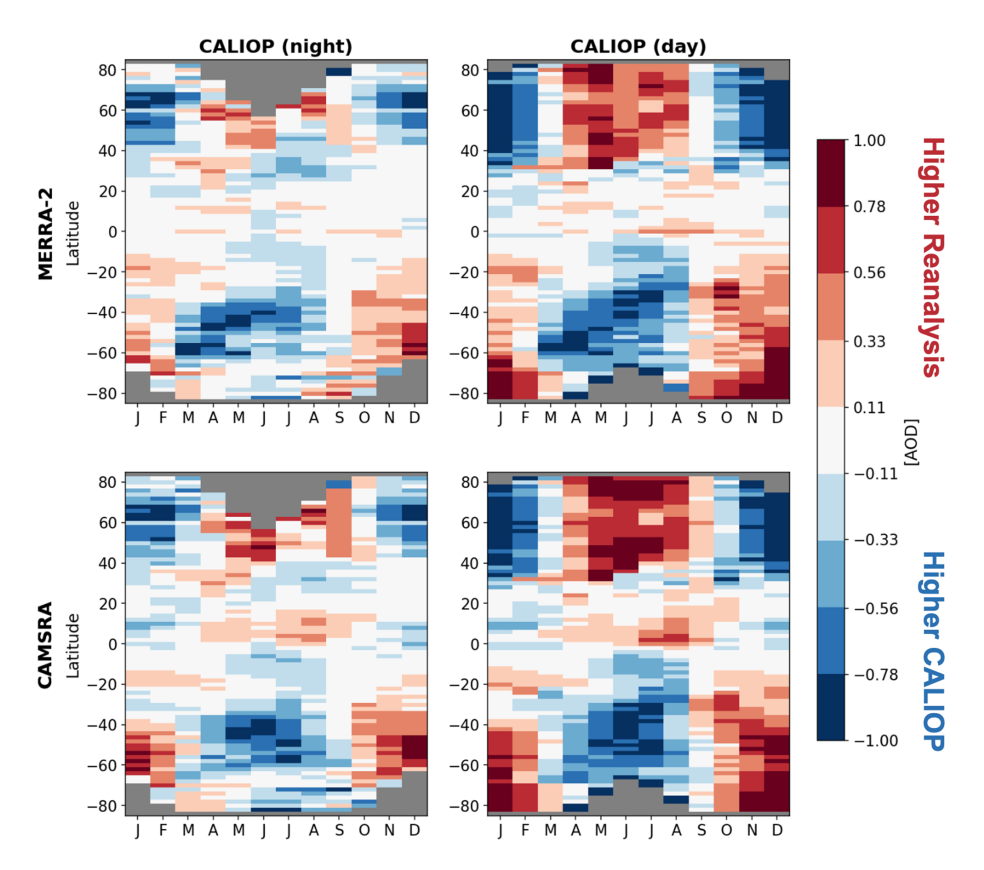


Figure 6. For each latitudinal band, monthly median zonal mean CALIOP (night and day) and reanalysis (MERRA-2 and CAMSRA) AODs were each normalized to their respective seasonal cycles. The difference between the normalized AODs ( $\tau_{\text{Reanalysis, normed}} - \tau_{\text{CALIOP, normed}}$ ) with regards to latitude and month is shown, for each CALIOP (day and night) and reanalysis (MERRA-2 and CAMSRA) pair.

or magnitude of the effect of the all-RFV profiles varies with the SZA.

A-train overpasses during lower SZAs occur in the low and midlatitudes, making an examination of the absolute difference in AOD unhelpful—absolute differences are likely to be greatest at latitudes where baseline AODs are also highest (e.g. midlatitude source regions). Thus, we expect that the greatest absolute differences in AOD would occur at SZAs observed during source region overpasses, regardless of any retrieval artifacts. Accordingly, for our analysis we consider a measure of relative difference, rather than an absolute difference in AOD, where the relative difference index (RDI) is defined:

$$RDI = \frac{\tau_{MOD} - \tau_{CAL}}{\tau_{MOD} + \tau_{CAL}} \tag{2}$$

This index is the difference between the instruments relative to the instrument-mean, normalized to a range of  $\pm 1$ . For colocations in which MODIS is greater, the index will be positive, while in instances in which CALIOP is greater the sign will be negative. As neither instrument serves as a ground-truth reference, we normalize to the mean of the two instruments rather than to either individually.

However, the RDI should only be applied to colocations in which both instruments retrieve positive values of AOD. In CALIOP all-RFV profiles (which Toth et al., 2018, found account for 71 % of daytime AODs), the relative difference index will always return a value of -1 for any positive valued MODIS colocation, regardless of its magnitude. Meanwhile, negative or zero-valued MODIS AODs could result in a relative difference that is undefined, or outside the  $\pm 1$  range. Accordingly, we consider two different cases:

- 1. the all-positives case, in which both instruments retrieve positive values of AOD
- 2. the zeroes case, in which one instrument retrieves an AOD of zero or less, and the other instrument retrieves some positive value of AOD

This approach has the additional benefit of allowing us to consider whether the impact of CALIOP all-RFV retrievals vary with the SZA, which can provide insight into whether this well-known mechanism by which CALIOP underreports AOD exhibits an SZA dependency. Finally, we consider whether the correlation between the colocated CALIOP and MODIS AODs depends on the SZA, which offers data users insight into the utility of different datasets under different SZA conditions.

## 4.2.1 The all-positives case

We found that in 105 873 of the 138 866 colocations (76.2%) identified in Sect. 3.2, both instruments returned positive values of AOD. Figure 7 shows kernel density estimates (KDEs) of the RDI with respect to the cosine of the SZA, for all nonzero colocations (Fig. 7a), as well as for subsets in which MODIS retrievals are assigned high-quality ("3") and low-quality ("1") QAC flags (Fig. 7b and c, respectively). A linear regression of the form:

$$RDI = m \cdot \cos(\theta) + b \tag{3}$$

is overlaid on each subplot, where the slope (m) describes the sensitivity of the RDI to the SZA  $(\theta)$ . As the RDI is 1/2 the bias divided by the mean of both instruments, multiplying the slope by 200 (i.e.,  $2 \times 100$ ) yields the percent change  $(\%\Delta)$  in bias relative to the instrument-mean over a unit change in  $\cos(\theta)$  – equivalent to a shift from 0 to 90° SZA. To calculate the percent change over a specific SZA range  $(\%\Delta_{\theta_0\to\theta_1})$ , this value can be further multiplied by the difference in  $\cos(\theta)$  between the lower and upper bounds of that range, as described below:

$$\%\Delta_{\theta_0 \to \theta_1} = m \cdot [\cos(\theta_0) - \cos(\theta_1)] \cdot 200 \tag{4}$$

Both m and  $(\%\Delta_{0\rightarrow 90})$  are shown in Table 1. Across all all-positives cases, a substantial decrease in the RDI with increasing SZAs is evident (Fig. 7a). The dependency accounts for a  $\%\Delta_{0\rightarrow 90}$  of -97%. This negative  $\%\Delta_{0\rightarrow 90}$  indicates that MODIS AODs are declining as the SZA increases, without a commensurate reduction in CALIOP AODs, or that CALIOP AODs are increasing with higher SZAs, without a similar effect on MODIS retrievals (a combination of both reduced MODIS and increased CALIOP AODs is also possible).

Subsets characterized by high- and low-quality MODIS retrievals (Fig. 7b and c, respectively) also show significant negative dependencies on the SZA, though the dependency for the subset characterized by low-quality MODIS retrievals is far more substantial, accounting for a  $\%\Delta_{0\rightarrow90}$  of -132%, as opposed to just -33% for the high-quality subset (Table 1). In addition, standard errors from the calculated dependency are less for colocations characterized by low-(SE = 0.0074) versus high- (SE = 0.011) quality MODIS retrievals (Table 1), which is apparent in the greater concentration of the KDE around the regression line in Fig. 7c. The dependency also explains substantially more variance ( $R^2$ , Table 1) among the subset of low- (nearly 14%) versus high-(less than 0.5%) quality MODIS retrievals, as well as the set of all retrievals ( $\cong$  6%).

In our set of all-positive colocations, most (85%) occurred over the ocean. No over-land MODIS retrievals were assigned a low-quality flag, and few occurred at  $> 60^\circ$  SZA (Fig. S1). Colocations with high-quality MODIS retrievals that occurred over the ocean (Fig. S2) showed slight negative dependencies with the SZA, while those that occurred

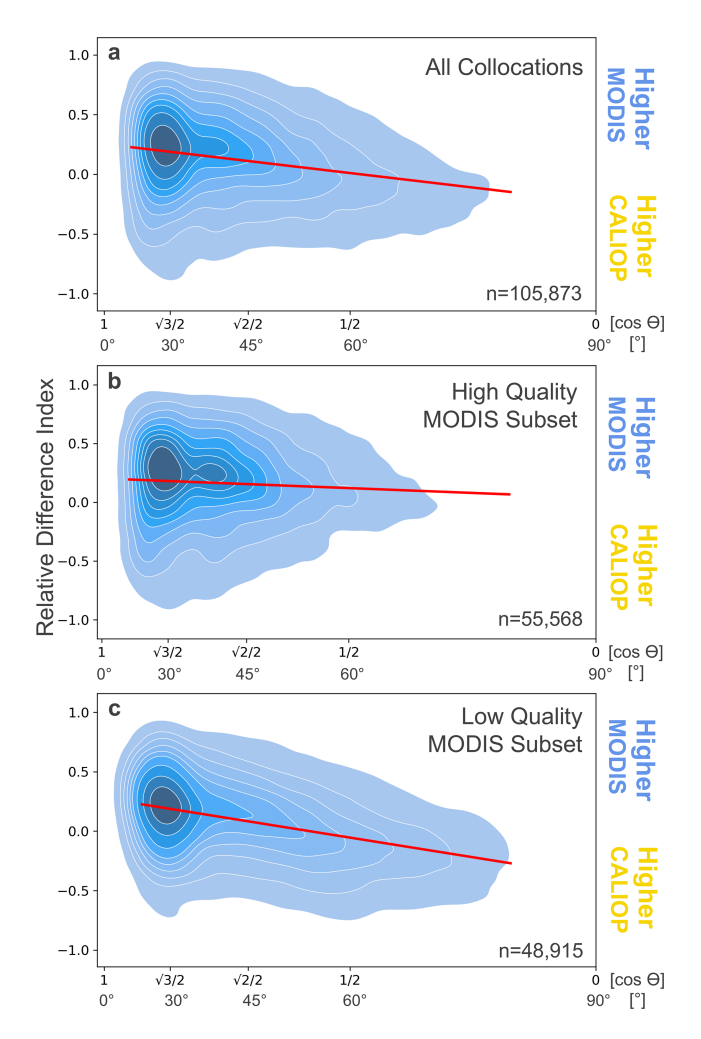


Figure 7. (a) A kernel density estimate (KDE) of the relative difference index [(MODIS-CALIOP)/(MODIS+CALIOP)] between all non-zero MODIS and CALIOP retrievals as a function of the cosine of the SZA; a linear regression to the cosine of the SZA is also shown (red). (b) Same as a, except for only colocations with high ("3") MODIS QAC flags. (c) Same as (a), except for only colocations with low ("1") MODIS QAC flags.

over land were slightly positive, though in both cases the dependency was low in magnitude, and with much greater SEs than we observe in the low-quality MODIS subset. The low-quality MODIS subset (Fig. 7c) is therefore characterized exclusively by retrievals over the ocean. That the dependency is substantially more robust within this subset of colocations indicates that MODIS retrieval quality plays a considerable role in mediating the observed dependency. Conversely, the relatively minimal effect in the subset with high-quality MODIS retrievals suggests that both CALIOP and high-quality MODIS retrievals are affected relatively little by the SZA, and points instead to the low-quality MODIS retrievals being primarily sensitive to changes in the SZA.

The KDE corresponding to the set of all all-positive colocations (Fig. 7a) contains roughly equal contributions from

**Table 1.** The slope (m), p value (p), variance explained  $(R^2)$ , standard error (SE), number of colocations (n), and percent difference in AOD (relative to the instrument-mean) over a 0 to 90° SZA range for linear regressions corresponding to KDEs shown in Fig. 7. Values are shown for all all-positive colocations (Fig. 7a), and for subsets characterized by high and low MODIS QAC flags (Fig. 7b and c, respectively). Indications of p=0 occur when p-values were less than could be calculated with a 64-bit float.

	All	High QAC	Low QAC
m	-0.48619	-0.16467	-0.66154
p	0	$5.863 \times 10^{-53}$	0
$R^2$	0.05670	0.00421	0.13828
SE	0.00627	0.01074	0.00747
n	105 873	55 568	48 915
$\%\Delta_{0\rightarrow90}$	-97%	-33 %	-132%

the low (48 915) and high (55 568) quality MODIS retrievals. However, as seen in Fig. 3, MODIS retrieval quality shows distinct patterns of spatiotemporal variability, with lower (higher) quality retrievals more prevalent in months and latitudes characterized by higher (lower) SZAs. Thus, the KDE corresponding to the set of all colocations (Fig. 7a) better resembles the high-quality MODIS subset (Fig. 7b) at lower SZAs, and the low-quality MODIS subset (Fig. 7c) at higher SZAs.

In the low-quality MODIS subset (Fig. 7c), the dependency is apparent even at low SZAs. This finding suggests that the mechanism by which the dependency occurs is not simply an artifact of increasingly poor data quality at very high SZAs. Rather, it is evident at all SZAs when data quality is low, but masked by the higher fraction of high-quality retrievals at low SZAs. Thus, in the L3 gridded product, averaging schemes likely dampen the effect of the dependency until the fraction of high-quality retrievals is substantially diminished.

Like other passive sensor data sets, the MODIS L3 AOD product shows divergent seasonality from CALIOP in the high latitudes (>  $60^{\circ}$  N) (Fig. 5). Using the equation for  $\%\Delta_{\theta_0\to\theta_1}$  described above, we predict a  $\sim 78\,\%$  decline in low-quality MODIS Arctic retrievals in winter versus summer, relative to the instrument-mean, using summer and winter SZAs of 40 and  $80^{\circ}$ , respectively (consistent with average June and January SZAs at  $60^{\circ}$  N at 13:00, near the A-train overpass time). Given the high prevalence of low-quality retrievals in this season, this relationship offers a compelling explanation for the observed differences in seasonality, though CALIOP sensitivity must still be considered and data quality across SZAs more precisely characterized.

## 4.2.2 The zeroes case

In 25 226 of the 138 866 colocations (18%), one instrument retrieved an AOD of zero (or less) and another retrieved a

positive value of AOD. A tendency for the CAD in CALIOP processing to classify optically thin aerosol layers as clean air drives the low bias in CALIOP AODs relative to MODIS, globally; a lower SNR for CALIOP retrievals during the day results in an enhancement of this bias (Kim et al., 2017; Toth et al., 2018). Thus, one hypothetical mechanism by which active versus passive sensor AOD biases may depend on the SZA is that the active sensor SNR may decrease with higher SZAs, resulting in a reduction in the incidence of "undetected layers", and, accordingly, all-RFV profiles. To date, no studies have examined the frequency of CALIOP all-RFV profiles against the SZA. Cases in which CALIOP retrieves an AOD of zero, but MODIS retrieves a positive value of AOD, indicate that the column is subject to one or more such undetected layers. By examining the frequency of such cases, we can also determine whether this well-known source of bias depends on the SZA.

Accordingly, we define the "zeroes case" as colocations in which one instrument retrieves an AOD of zero or less, while the other instrument retrieves some positive value. For brevity, we refer to instances in which CALIOP retrieves an AOD of zero, and MODIS retrieves a positive value of AOD, as the "CALIOP-zero" case, and instances in which MODIS returns a value of zero or less and CALIOP returns a positive value as the "MODIS-zero" case. CALIOP-zero cases will contribute to relatively higher average MODIS AODs, while MODIS-zero cases will contribute towards relatively higher average CALIOP AODs.

Figure 8 shows the fraction of colocations within 5° SZA bins characterized by MODIS-zero (yellow bars) and CALIOP-zero (blue bars) cases; the MODIS-zero fractions are assigned a positive value, while the CALIOP-zero fractions are assigned a negative value, in accordance with the sign of their contributions to the bias (defined as  $\tau_{\text{MODIS}} - \tau_{\text{CALIOP}}$ ) (left y axis). To assess the contribution of each case to SZA-averaged AODs, we calculate the mean difference with the colocated positive-valued AODs within each bin and for each instrument. We then multiply these values by the corresponding fraction of zeroes-biased retrievals, for both MODIS- and CALIOP-zero cases; these calculations give the contribution of each case to the bias, while their sum gives the effect of all zeroes cases in total, within each SZA bin.

For SZAs bins between 20 and 80°, CALIOP-zero cases occur in 9 %–23 % of colocations, a substantial fraction of the total number of colocations. However, the incidence of the CALIOP-zero cases shows no monotonic relationship with the SZA. In contrast, from 20–50° SZA MODIS-zero cases consistently make up fewer than 2 % of colocations. However, beginning at 50–55° SZA, the incidence of the MODIS-zero case rises exponentially, from 1.7 % at 50–55° to 13 % at 75–80° SZA. The exceptionally high (67 %) fraction of MODIS-zero cases in the 80–85° SZA bin was calculated from only three total colocations, all of which were retrieved at less than 81° SZA.

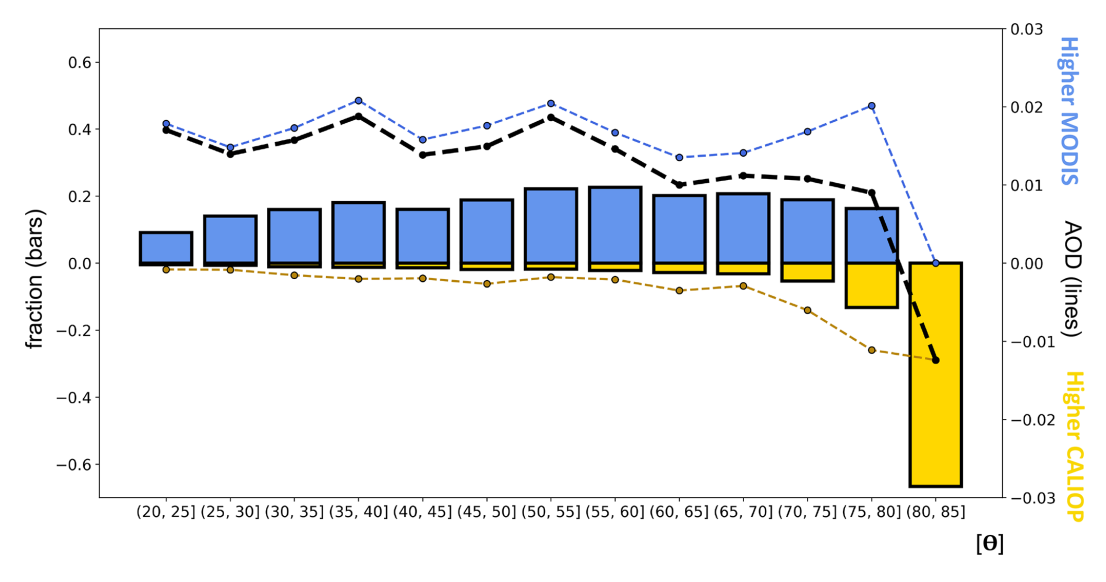


**Figure 8.** The fraction (left y axis) of colocations corresponding to CALIOP-zero (blue bars) or MODIS-zero (yellow bars) cases, and the contribution (right y axis) of MODIS-zero (yellow, dashed line) and CALIOP-zero (blue, dashed line) cases to the bias within each  $5^{\circ}$  solar zenith angle bin. The sum of the contributions from both instruments (black, dashed line) is shown in black, and shows the total contribution from all zeroes cases to the bias between instruments within each  $5^{\circ}$  solar zenith angle bin.

These findings indicate that MODIS is susceptible to falsely retrieving AODs of zero or less as the SZA increases above moderately high (50–55°) angles. CALIOP is also susceptible to falsely retrieving AODs of zero, and does so more frequently than MODIS in all SZA bins below 80°. However, the frequencies of CALIOP-zero cases do not depend on the SZA, while those of the MODIS-zero cases do.

From 20–80° SZAs, CALIOP-zero cases consistently contribute between 0.0135 and 0.0208 to the bias, which is slightly less than the bias from undetected layers (0.031  $\pm$  0.052) found by Kim et al. (2017). As our analysis considers only the contribution of undetected layers resulting in a total column AOD of zero, we expect the CALIOP-zero contribution to be slightly less than the Kim et al. (2017) estimate.

Below 55° SZA, the impact of MODIS-zero cases is small when compared to the contributions from CALIOPzero cases (Fig. 8). From 60-65° SZA, MODIS-zero cases contribute -0.00352 to the bias, offsetting 26 % of the contribution (0.0135) from CALIOP-zero cases; from 70-75° SZA MODIS-zero cases offsets more than a third (36%) of the bias from CALIOP-zero cases, while from 75-80° SZA it offsets 55%. Thus, as the SZA increases above 50-55°, MODIS-zero cases increasingly offset the effects of CALIOP-zero cases. Our analysis indicates that the frequency of CALIOP all-RFV profiles does not vary substantially with the SZA, but conditions leading to MODIS retrievals of zero or less do. Thus, differences in the frequency of undetected layers likely contribute little to observed differences in CALIOP versus MODIS Arctic AOD seasonality; instead, MODIS increasingly fails to detect positive AOD values as the SZA increases over 50°.

As mentioned in Sect. 2.4, some negative MODIS AODs are expected when AODs are low, since negative values fall within an expected error envelope. A simple increase in the frequency of negative or zero-valued retrievals would be expected at locations and times where aerosol burdens are characteristically low, and these retrievals may coincide with higher SZAs. However, "MODIS zero" cases as defined above are only identified when CALIOP (which is known to "miss" optically thin AODs) returns positive values. Thus, it seems likely that MODIS is reporting artificially low AODs at high SZAs when column aerosol is non-negligible, consistent with our findings in Sect. 4.2.1.

In Sect. 4.2.1, we found that a pronounced SZA dependency was evident in colocations characterized by lowquality MODIS retrievals, but colocations characterized by high-quality MODIS retrievals showed minimal effects. In this section, we find that instances in which MODIS retrieves an AOD of zero or less increase with the SZA, whereas CALIOP all-RFV profiles do not. Together, these results demonstrate that low-quality MODIS retrievals, which are more prevalent in latitudes and months characterized by high SZAs (Fig. 3), likely drive most of the observed dependency. Still, a more quantitative measure of MODIS retrieval quality at different SZAs is necessary to understand the effects of the dependency on L3 average AODs in the high latitudes. Moreover, for many data users, the usefulness of AOD measures depends less on dataset biases, and more on whether datasets detect various aerosol events. While we have determined that the bias between datasets may depend on the SZA, it remains undetermined whether the correlation between CALIOP and MODIS AODs varies with the SZA.

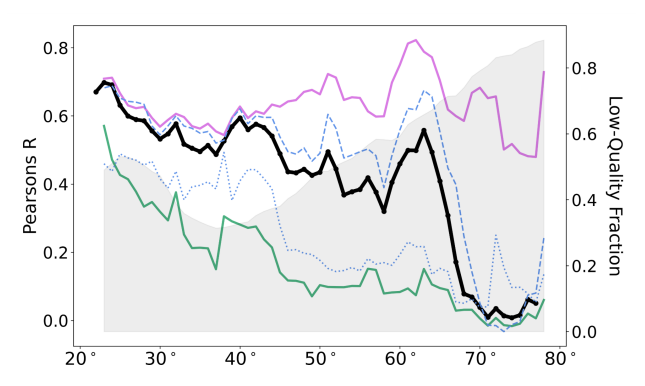


**Figure 9.** Pearson's R for colocated MODIS and CALIOP AODs within running  $5^{\circ}$  SZA bins (left y axis), for all colocations (black line), colocations with high-quality MODIS retrievals (purple solid line), colocations with low-quality MODIS retrievals (green solid line), NH colocations (dashed blue line), and SH colocations (blue dotted line). The fraction of colocations within each running  $5^{\circ}$  SZA bin characterized by low-quality MODIS retrievals is shown by the gray shading (right y axis).

# 4.2.3 Usefulness of low-quality retrievals

In remote regions where observations are sparse, extracting as much information as possible from all available data sources is compelling. In many cases, imperfect or incomplete data can provide useful information, but only when the biases and limitations of the data are understood.

Validation of AOD data products involves assessing both the bias and the correlation between instruments. Bias provides important context for interpreting differences between the instrument retrievals, while correlation determines whether the data capture similar phenomena. Above, we examined whether the bias between CALIOP and MODIS products depends on the SZA. Now, we consider whether the correlation shows similar dependencies.

To determine whether the SZA affects the correlation between CALIOP and MODIS, we calculated Pearson's R for the above colocations within running  $5^{\circ}$  SZA bins (Fig. 9, black line). To examine the extent to which retrieval quality and hemispheric location intervene in this relationship, we performed the same analysis for subsets of colocations characterized by high- (purple line) and low- (green line) quality MODIS retrievals, and separately for subsets from the NH (blue dashed line) and SH (blue dotted line). The fraction of colocations within each  $5^{\circ}$  SZA bin characterized by low-quality MODIS retrievals is shaded in gray (left y axis).

The correlations for all colocations (black line) show a pronounced negative SZA dependency, beginning at even low (25°) SZAs. A brief departure from the overall negative relationship begins at  $58^{\circ}$  and peaks at  $65^{\circ}$  SZA, with R nearly doubling from 0.340 to 0.570. The departure is followed by a precipitous drop in correlation at increasingly high ( $68^{\circ}$ ) SZAs. This temporary increase in correlation is evident in colocation subsets characterized by NH coloca-

tions and high-quality MODIS retrievals, but not SH colocations or low-quality MODIS retrievals. Retrievals with SZAs between 58 and 65° in the NH correspond to midlatitude source regions, and enhanced correlation likely stems from higher average AODs (and hence greater variability), and perhaps better constraints on retrieval processing in more accessible regions.

Across all SZAs, the subset of colocations with high-quality MODIS retrievals shows no monotonic relationship to the SZA. For this subset, R remains consistently high at all SZAs, ranging from 0.512 to 0.828. In contrast, the subset characterized by low-quality MODIS retrievals shows lower correlations than the high-quality subset at virtually all SZAs, as well as a pronounced, steady decline in correlation with increasing SZAs. At low (< 22°) SZAs, low-quality MODIS retrievals are suitably correlated with their CALIOP counterparts (R > 0.5). Above moderate (> 45°) SZAs, the correlation never surpasses R = 0.3, while above 75° the correlation effectively disappears as R never exceeds 0.1.

From 40°, the fraction of colocations characterized by low-quality MODIS retrievals increases steadily with higher SZAs. Accordingly, the decline in correlation among all colocations is more pronounced than for just the low-quality MODIS retrieval subset, reflecting both the SZA dependency for low-quality MODIS retrievals, and the increased fraction of low-quality retrievals with higher SZAs. Similar to our findings in Sect. 4.2.1, the decline in correlation does not simply result from a decline in retrieval quality alone; it is evident at all SZAs among low-quality retrievals, and the increased incidence of low-quality retrievals at higher SZAs amplifies the relationship when averaging across all colocations.

The decline in correlation is evident in colocations from both the NH and SH, though SH colocations (blue, dotted line) are less correlated than NH correlations (blue, dashed line) at all SZAs below 70°, and do not show the abrupt decoupling at 65°. Instead, a more modest decline is observed after 42° SZA. SH retrievals with SZAs of 45° to 60° occur most frequently over the Southern Ocean, where MODIS retrievals are characteristically low-quality (Fig. 3). Accordingly, hemispheric differences in the relationship between correlation and the SZA can be explained by slight differences in the spatiotemporal variability of data quality. In both hemispheres, CALIOP and MODIS low-quality retrievals gradually decouple as the SZA increases, and the prevalence of low-quality MODIS retrievals intervenes in the relationship between correlation and SZA.

At SZAs greater than 60°, low-quality MODIS retrievals make up 60% or more of the retrievals, while at very high (> 70°) SZAs, MODIS retrievals are overwhelmingly (> 80%) low-quality. At 13:00 local time, SZAs at 60° N range from approximately 70° in late February to over 80° in mid-December, suggesting that wintertime Arctic retrievals from MODIS (Aqua) are mostly low-quality, and hence strongly influenced by the dependency described in Sect. 4.2.1.

The low correlation between CALIOP and MODIS retrievals at high SZAs indicates that the L3 data products become increasingly less likely to capture similar aerosol events at high SZAs, even apart from any effects on bias. Had the bias, but not correlation, shown an SZA dependency, data products in the high latitudes may be relied upon to show similar sub-seasonal variability, and similar interannual variability for a given month, even while the seasonality diverged. However, our findings indicate that the MODIS L3 products have limited utility when a preponderance of the gridcell-averaged L2 retrievals occur at SZAs above 63°. However, where sufficient coverage with high-quality L2 MODIS AODs is available, such retrievals may provide useful information even under very high (> 70°) SZAs.

## 5 Summary and Conclusion

The Arctic is characterized by both heightened sensitivity to radiative forcing and a paucity of observational constraints. As such, satellite data products have the potential to provide valuable information about the region, but only if their capabilities and limitations in the region are understood and, ideally, quantified. In this analysis, we found stark differences in Arctic AOD seasonality between CALIOP and six passive sensor L3 data products, even when controlling for sampling biases, with all passive sensor products reporting dubiously low AODs from early autumn to mid-spring. We further found that seasonal biases between CALIOP and two reanalysis products were evident in both hemispheres, extending from the poles into the midlatitudes. These findings suggest that biases in passive sensor AOD retrievals may be propagated into reanalysis products, as these datasets assimilate passive sensor observations. However, further investigation of the reanalysis products, including their assimilation and modeling processes, is needed to determine whether this is the case.

Our analysis of colocated L2 MODIS and CALIOP retrievals shows that the interplay between reduced MODIS retrieval quality in winter and a strong solar zenith angle dependence in low-quality retrievals substantially contributes to seasonality biases between passive and active sensor data products. Specifically, we can infer that the relationship is responsible for a  $\sim$  78 % reduction in over  $\sim$  80 % of MODIS high latitude retrievals in winter, compared to what they would be in the summer, relative to the instrument-mean. As noted in Sect. 2.4.2, QAC flag assignments do not depend explicitly on retrieval geometry, and indeed some high-quality retrievals are still present even at very high SZAs. Moreover, high-quality retrievals show little sensitivity to SZA, even at extreme angles (Fig. 7b). Therefore, retrieval quality is not fully explained by increasing SZAs, nor is the decline in AOD at high SZAs independent of retrieval quality. Rather, it is the interaction between declining quality and a

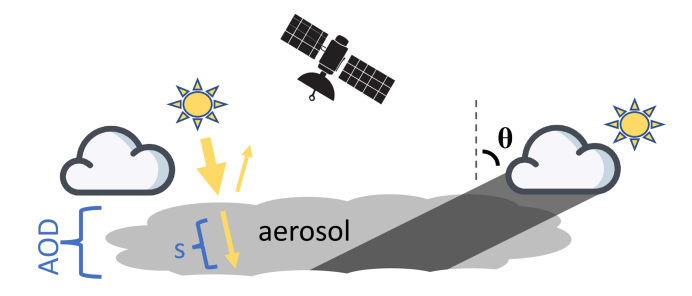


**Figure 10.** A schematic illustration of insolation and reflectance at low (left) and high (right) solar zenith angles ( $\theta$ ), with nearby clouds. At high SZAs, adjacent clouds may enshadow the aerosol layer, resulting in lower reflectance and underestimates of AOD for passive sensors. At low SZAs, the light source is unimpeded by neighboring clouds.

quality-mediated SZA dependence that drives the seasonal decoupling.

In addition, we demonstrate that other plausible explanations account for only a small fraction of the observed bias between instruments. Sampling bias is not sufficient to explain the observed differences (Fig. 5), and our analysis of CALIOP RFVs suggests that the instrument's sensitivity is not affected by the SZA (Fig. 8). Further, retrievals in the low-quality subset of data occurred over the ocean, where MODIS radiative transfer assumes a pseudospherical atmosphere, indicating that errors do not arise from the breakdown of plane-parallel assumptions. The lack of a strong trend in high-quality MODIS data (Fig. 7b) suggests that SZA-dependent biases stem primarily from low-quality MODIS retrievals, not CALIOP lidar ratio errors.

Still, outstanding questions remain. Our evaluation includes only passive sensor retrievals where the VZA was near-nadir; other works have shown that VZAs can affect MODIS cloud optical depths, and a VZA dependence for AOD is plausible as well. VZA variability changes little with the seasons in the Arctic, so it is unlikely to impact AOD seasonality on its own (Fig. S3). However, non-linear effects between SZA- and VZA-mediated biases are very possible, and need to be evaluated in order to understand the full effects of retrieval geometry on L3 datasets.

Next, the specific conditions responsible for this relationship have yet to be fully described. As described in Sect. 2.4.2, low-quality scores over ocean may be assigned due to a number of different retrieval characteristics, and we don't yet know whether the SZA-dependence is evident in all low-quality retrievals. One well-known source of uncertainty in remote sensing is cloud adjacency, whereby shadows or scattered light from neighboring clouds introduce unconstrained effects on reflectance measures in nearby pixels (see Fig. 10). Assessing how different pathways to low QAC scores vary in prevalence and SZA dependence will help clarify the role of this and other 3D artifacts. Better constraints on cloud adjacency could prove especially valuable, as more

reliable observations of aerosols near clouds could provide important insight into aerosol-cloud microphysical interactions, a topic of considerable importance to atmospheric and climate science.

Finally, for low-quality retrievals we found an SZA dependence in both biases and correlations, suggesting the potential for bias correction or more detailed error characterization in future products. Inversion algorithms for MODIS depend on measured top-of-atmosphere reflectance and assumptions about surface reflectance, path reflectance, and multiple scattering. While our analysis shows that CALIOP sensitivity does not appear to vary with SZA, ground-truth measures are necessary to provide important constraints on these assumptions under different retrieval geometries. Further comparisons of satellite AODs to AERONET, MAN, and ground-based lidar across a range of SZAs can help disentangle the effects of 3D artifacts on these different assumptions, and should be a focus of future investigations. Additionally, examining low-quality retrieval errors within different SZA and VZA bins can help determine the extent to which expected errors may vary with retrieval geometry, supporting more refined uncertainty quantification in future products.

In the meantime, high-quality L2 passive sensor retrievals may offer a useful alternative for studying Arctic AOD seasonality, though only when sampling biases are well-controlled. Complementary efforts to characterize Arctic aerosol variability are necessary to assess how well high-quality retrievals capture the range of aerosol conditions in the region, and to better understand the various processes shaping Arctic aerosol.

Data availability. L3 **MODIS** products from (https://doi.org/10.5067/MODIS/MYD04\_L2.061; 2015), **CALIOP** al.. (https://doi.org/10.5067/CALIOP/CALIPSO/CAL\_LID\_L3\_ Tropospheric\_APro\_AllSky-Standard-V4-20; NASA/LARC/SD/ASDC, VIIRS 2019), and (https://doi.org/10.5067/VIIRS/AERDB\_M3\_VIIRS\_SNPP.011; NASA Earth Data, 2025), and L2 products from CALIOP (https://doi.org/10.5067/CALIOP/CALIPSO/LID\_L2\_05KMAPRO-STANDARD-V4-20; NASA/LARC/SD/ASDC, 2018) and MODIS (https://doi.org/10.5067/MODIS/MYD04\_L2.061; Levy et al., 2015) can be downloaded from NASA's Atmospheric Science Data Center at Langley Research Center, while the SeaWiFS data product (https://doi.org/10.5067/MEASURES/SWDB/DATA304; Hsu et al., 2013b) is stored at NASA Goddard Space Flight Center. POLDER (https://www.grasp-open.com/products/ polder-data-release/, last access: 17 March 2020) can be accessed through AERIS/ICARE Data and Services Center. AVHRR (https://doi.org/10.7289/V5X9287S; Foster et al., 2021) can be accessed through the National Centers for Environmental Information (NCEI) at NOAA. MERRA2 (https://doi.org/10.5067/2E096JV59PK7; Global Modeling and Assimilation Office, 2015) can be accessed through the NASA Global Modeling and Assimilation Office. CAMS reanalysis

product (Inness et al., 2019) are available from the Copernicus Atmospheric data store.

**Supplement.** The supplement related to this article is available online at https://doi.org/10.5194/acp-25-14333-2025-supplement.

**Author contributions.** SS developed the hypothesis, methodology, and performed the investigation of this analysis, with feedback and suggestions from YW and MT and RL. YW and MT helped conceptualize methods for controlling for sampling biases in results Sect. 4.1, while RL provided feedback on data products, suggested partitioning colocations by QAC flag in Sect. 4.2, and provided feedback on explanatory mechanisms to describe the observed findings. SS wrote the original manuscript, with edits from RL, YW, and MT.

**Competing interests.** The contact author has declared that none of the authors has any competing interests.

**Disclaimer.** Publisher's note: Copernicus Publications remains neutral with regard to jurisdictional claims made in the text, published maps, institutional affiliations, or any other geographical representation in this paper. While Copernicus Publications makes every effort to include appropriate place names, the final responsibility lies with the authors. Also, please note that this paper has not received English language copy-editing. Views expressed in the text are those of the authors and do not necessarily reflect the views of the publisher.

**Acknowledgements.** The authors would like to thank Earth Science Senior 80 Review: Terra and Aqua Algorithm Maintenance.

**Financial support.** This research has been supported by the Office of Polar Programs (grant no. OPP-1825858) and the Earth Sciences Division (grant no. 80NSSC20K1254).

**Review statement.** This paper was edited by Matthew Christensen and reviewed by Lorraine Remer and two anonymous referees.

#### References

AMAP Assessment 2015: Black carbon and ozone as Arctic climate forcers | AMAP: https://www.amap.no/documents/doc/amap-assessment-2015-black-carbon-and-ozone-as-arctic-climate-forcers/1299, last access: 18 July 2024.

Bintanja, R. and Krikken, F.: Magnitude and pattern of Arctic warming governed by the seasonality of radiative forcing, Sci. Rep., 6, 38287, https://doi.org/10.1038/srep38287, 2016.

- Buchard, V., Randles, C. A., Da Silva, A. M., Darmenov, A., Colarco, P. R., Govindaraju, R., Ferrare, R., Hair, J., Beyersdorf, A. J., Ziemba, L. D., and Yu, H.: The MERRA-2 Aerosol Reanalysis, 1980 Onward. Part II: Evaluation and Case Studies, J. Climate, 30, 6851–6872, https://doi.org/10.1175/JCLI-D-16-0613.1, 2017.
- Chen, C., Dubovik, O., Fuertes, D., Litvinov, P., Lapyonok, T., Lopatin, A., Ducos, F., Derimian, Y., Herman, M., Tanré, D., Remer, L. A., Lyapustin, A., Sayer, A. M., Levy, R. C., Hsu, N. C., Descloitres, J., Li, L., Torres, B., Karol, Y., Herrera, M., Herreras, M., Aspetsberger, M., Wanzenboeck, M., Bindreiter, L., Marth, D., Hangler, A., and Federspiel, C.: Validation of GRASP algorithm product from POLDER/PARASOL data and assessment of multi-angular polarimetry potential for aerosol monitoring, Earth Syst. Sci. Data, 12, 3573–3620, https://doi.org/10.5194/essd-12-3573-2020, 2020.
- Deschamps, P.-Y., Breon, F.-M., Leroy, M., Podaire, A., Bricaud, A., Buriez, J.-C., and Seze, G.: The POLDER mission: instrument characteristics and scientific objectives, IEEE Trans. Geosci. Remote Sensing, 32, 598–615, https://doi.org/10.1109/36.297978, 1994.
- Diner, D. J., Beckert, J. C., Reilly, T. H., Bruegge, C. J., Conel, J. E., Kahn, R. A., Martonchik, J. V., Ackerman, T. P., Davies, R., Gerstl, S. A. W., Gordon, H. R., Muller, J., Myneni, R. B., Sellers, P. J., Pinty, B., and Verstraete, M. M.: Multi-angle Imaging SpectroRadiometer (MISR) instrument description and experiment overview, IEEE Trans. Geosci. Remote Sensing, 36, 1072–1087, https://doi.org/10.1109/36.700992, 1998.
- Di Pierro, M., Jaeglé, L., Eloranta, E. W., and Sharma, S.: Spatial and seasonal distribution of Arctic aerosols observed by the CALIOP satellite instrument (2006–2012), Atmos. Chem. Phys., 13, 7075–7095, https://doi.org/10.5194/acp-13-7075-2013, 2013.
- Dubovik, O., Herman, M., Holdak, A., Lapyonok, T., Tanré, D., Deuzé, J. L., Ducos, F., Sinyuk, A., and Lopatin, A.: Statistically optimized inversion algorithm for enhanced retrieval of aerosol properties from spectral multi-angle polarimetric satellite observations, Atmos. Meas. Tech., 4, 975–1018, https://doi.org/10.5194/amt-4-975-2011, 2011.
- Dubovik, O., Lapyonok, T., Litvinov, P., Herman, M., Fuertes, D., Ducos, F., Torres, B., Derimian, Y., Huang, X., Lopatin, A., Chaikovsky, A., Aspetsberger, M., and Federspiel, C.: GRASP: a versatile algorithm for characterizing the atmosphere, SPIE Newsroom, https://doi.org/10.1117/2.1201408.005558, 2014.
- Dubovik, O., Fuertes, D., Litvinov, P., Lopatin, A., Lapyonok, T.,
  Doubovik, I., Xu, F., Ducos, F., Chen, C., Torres, B., Derimian,
  Y., Li, L., Herreras-Giralda, M., Herrera, M., Karol, Y., Matar,
  C., Schuster, G. L., Espinosa, R., Puthukkudy, A., Li, Z., Fischer, J., Preusker, R., Cuesta, J., Kreuter, A., Cede, A., Aspetsberger, M., Marth, D., Bindreiter, L., Hangler, A., Lanzinger,
  V., Holter, C., and Federspiel, C.: A Comprehensive Description of Multi-Term LSM for Applying Multiple a Priori Constraints in Problems of Atmospheric Remote Sensing: GRASP Algorithm, Concept, and Applications, Front. Remote Sens., 2, 706851, https://doi.org/10.3389/frsen.2021.706851, 2021.
- Eckhardt, S., Quennehen, B., Olivié, D. J. L., Berntsen, T. K., Cherian, R., Christensen, J. H., Collins, W., Crepinsek, S., Daskalakis, N., Flanner, M., Herber, A., Heyes, C., Hodnebrog, Ø., Huang, L., Kanakidou, M., Klimont, Z., Langner, J., Law,

- K. S., Lund, M. T., Mahmood, R., Massling, A., Myriokefalitakis, S., Nielsen, I. E., Nøjgaard, J. K., Quaas, J., Quinn, P. K., Raut, J.-C., Rumbold, S. T., Schulz, M., Sharma, S., Skeie, R. B., Skov, H., Uttal, T., von Salzen, K., and Stohl, A.: Current model capabilities for simulating black carbon and sulfate concentrations in the Arctic atmosphere: a multi-model evaluation using a comprehensive measurement data set, Atmos. Chem. Phys., 15, 9413–9433, https://doi.org/10.5194/acp-15-9413-2015, 2015.
- Foster, M. J., Phillips, C., Heidinger, A. K., and NOAA CDR Program: NOAA Climate Data Record (CDR) of Advanced Very High Resolution Radiometer (AVHRR) and Highresolution Infra-Red Sounder (HIRS) Reflectance, Brightness Temperature, and Cloud Products from Pathfinder Atmospheres – Extended (PATMOS-x), Version 6.0, NOAA National Centers for Environmental Information [data set], https://doi.org/10.7289/V5X9287S, 2021.
- Global Modeling and Assimilation Office (GMAO): MERRA-2 instM\_3d\_asm\_Np: 3d,Monthly mean,Instantaneous,Pressure-Level,Assimilation,Assimilated Meteorological Fields V5.12.4, Greenbelt, MD, USA, Goddard Earth Sciences Data and Information Services Center (GES DISC) [data set], https://doi.org/10.5067/2E096JV59PK7, 2015.
- Grosvenor, D. P. and Wood, R.: The effect of solar zenith angle on MODIS cloud optical and microphysical retrievals within marine liquid water clouds, Atmos. Chem. Phys., 14, 7291–7321, https://doi.org/10.5194/acp-14-7291-2014, 2014.
- Gueymard, C. A. and Yang, D.: Worldwide validation of CAMS and MERRA-2 reanalysis aerosol optical depth products using 15 years of AERONET observations, Atmospheric Environment, 225, 117216, https://doi.org/10.1016/j.atmosenv.2019.117216, 2020.
- Haas, C., Belhadj, T., Kruse, K.-W., De Villèle, G., Sauer, M., Chassat, F., Corselle, B., Tzeremes, G., Pereira Do Carmo, J., Ghose, K., and Wallace, K.: ATLID (ATmospheric lidar) integration and initial test results on EarthCARE satellite, in: International Conference on Space Optics – ICSO 2022, International Conference on Space Optics – ICSO 2022, Dubrovnik, Croatia, 53, https://doi.org/10.1117/12.2689292, 2023.
- Hsu, N. C., Jeong, M.-J., Bettenhausen, C., Sayer, A. M., Hansell, R., Seftor, C. S., Huang, J., and Tsay, S.-C.: Enhanced Deep Blue aerosol retrieval algorithm: The second generation, J. Geophys. Res.-Atmos., 118, 9296–9315, https://doi.org/10.1002/jgrd.50712, 2013a.
- Hsu, N. C., Sayer, A. M., Jeong, M.-J., and Bettenhausen, C.: SeaWiFS Deep Blue Aerosol Optical Depth and Angstrom Exponent Monthly Level 3 Data Gridded at 1.0 Degrees V004, Greenbelt, MD, USA, Goddard Earth Sciences Data and Information Services Center (GES DISC) [data set], https://doi.org/10.5067/MEASURES/SWDB/DATA304, 2013b.
- Hsu, N. C., Lee, J., Sayer, A. M., Carletta, N., Chen, S.-H., Tucker, C. J., Holben, B. N., and Tsay, S.-C.: Retrieving near-global aerosol loading over land and ocean from AVHRR, J. Geophys. Res.-Atmos., 122, 9968–9989, https://doi.org/10.1002/2017JD026932, 2017.
- Huang, L., Gong, S. L., Jia, C. Q., and Lavoué, D.: Importance of deposition processes in simulating the seasonality of the Arctic black carbon aerosol, Journal of Geophysical Research, 115, https://doi.org/10.1029/2009JD013478, 2010.

- Hubanks, Paul: MODIS Atmosphere QA Plan, Collection 6.1, https://atmosphere-imager.gsfc.nasa.gov/sites/default/files/ModAtmo/documents/QA\_Plan\_C61\_Master\_2021\_09\_22.pdf (last access: 6 July 2025), 2021.
- Inness, A., Ades, M., Agustí-Panareda, A., Barré, J., Benedictow, A., Blechschmidt, A.-M., Dominguez, J. J., Engelen, R., Eskes, H., Flemming, J., Huijnen, V., Jones, L., Kipling, Z., Massart, S., Parrington, M., Peuch, V.-H., Razinger, M., Remy, S., Schulz, M., and Suttie, M.: The CAMS reanalysis of atmospheric composition, Atmos. Chem. Phys., 19, 3515–3556, https://doi.org/10.5194/acp-19-3515-2019, 2019.
- Kim, M.-H., Omar, A. H., Vaughan, M. A., Winker, D. M., Trepte, C. R., Hu, Y., Liu, Z., and Kim, S.-W.: Quantifying the low bias of CALIPSO's column aerosol optical depth due to undetected aerosol layers: Undetected Aerosols in CALIPSO AOD, J. Geophys. Res. Atmos., 122, 1098–1113, https://doi.org/10.1002/2016JD025797, 2017.
- Kim, M.-H., Omar, A. H., Tackett, J. L., Vaughan, M. A., Winker, D. M., Trepte, C. R., Hu, Y., Liu, Z., Poole, L. R., Pitts, M. C., Kar, J., and Magill, B. E.: The CALIPSO version 4 automated aerosol classification and lidar ratio selection algorithm, Atmos. Meas. Tech., 11, 6107–6135, https://doi.org/10.5194/amt-11-6107-2018, 2018.
- Kittaka, C., Winker, D. M., Vaughan, M. A., Omar, A., and Remer, L. A.: Intercomparison of column aerosol optical depths from CALIPSO and MODIS-Aqua, Atmos. Meas. Tech., 4, 131–141, https://doi.org/10.5194/amt-4-131-2011, 2011.
- Levy, R. C., Remer, L. A., Mattoo, S., Vermote, E. F., and Kaufman, Y. J.: Second-generation operational algorithm: Retrieval of aerosol properties over land from inversion of Moderate Resolution Imaging Spectroradiometer spectral reflectance, J. Geophys. Res., 112, 2006JD007811, https://doi.org/10.1029/2006JD007811, 2007.
- Levy, R. C., Mattoo, S., Munchak, L. A., Remer, L. A., Sayer, A. M., Patadia, F., and Hsu, N. C.: The Collection 6 MODIS aerosol products over land and ocean, Atmos. Meas. Tech., 6, 2989–3034, https://doi.org/10.5194/amt-6-2989-2013, 2013.
- Levy, R., Hsu, C., Sayer, A., Mattoo, S., and Lee, J.: MODIS Atmosphere L2 Aerosol Product. NASA MODIS Adaptive Processing System, Goddard Space Flight Center, USA [data set], https://doi.org/10.5067/MODIS/MYD04\_L2.061, 2015.
- Levy, R. C., Sawyer, V., and Kiliyanpilakkil, P.: AL-GORITHM FOR REMOTE SENSING OF TRO-POSPHERIC AEROSOL OVER DARK TARGETS, https://darktarget\_gsfc.nasa.gov/sites/default/files/users/user9/ATBD\_DarkTarget\_April3.pdf (last access: 12 November 2024), 2024.
- Li, W., Su, X., Feng, L., Wu, J., Zhang, Y., and Cao, M.: Comprehensive Validation and Comparison of Three VIIRS Aerosol Products over the Ocean on a Global Scale, Remote Sensing, 14, 2544, https://doi.org/10.3390/rs14112544, 2022.
- Maddux, B. C., Ackerman, S. A., and Platnick, S.: Viewing Geometry Dependencies in MODIS Cloud Products, https://doi.org/10.1175/2010JTECHA1432.1, 2010.
- McCarty, J. L., Aalto, J., Paunu, V.-V., Arnold, S. R., Eckhardt, S., Klimont, Z., Fain, J. J., Evangeliou, N., Venäläinen, A., Tchebakova, N. M., Parfenova, E. I., Kupiainen, K., Soja, A. J., Huang, L., and Wilson, S.: Reviews and syntheses: Arctic fire

- regimes and emissions in the 21st century, Biogeosciences, 18, 5053–5083, https://doi.org/10.5194/bg-18-5053-2021, 2021.
- Mitchell, M.: Early identification of Arctic haze–reference to the Alaskan Arctic, Journal of Atmospheric and Terrestrial Physics Special Supplement, 195–211, 1956.
- Mölders, N. and Friberg, M.: Changes in Aerosol Optical Depth over the Arctic Ocean as Seen by CALIOP, MAIAC, and MODIS C6.1, JEP, 14, 419–440, https://doi.org/10.4236/jep.2023.146025, 2023.
- Munchak, L. A., Levy, R. C., Mattoo, S., Remer, L. A., Holben, B. N., Schafer, J. S., Hostetler, C. A., and Ferrare, R. A.: MODIS 3 km aerosol product: applications over land in an urban/suburban region, Atmos. Meas. Tech., 6, 1747–1759, https://doi.org/10.5194/amt-6-1747-2013, 2013.
- NASA/LARC/SD/ASDC: CALIPSO Level V4-20, Aerosol Profile, NASA Langley Atmo-Center DAAC spheric Science Data [data set], https://doi.org/10.5067/CALIOP/CALIPSO/LID\_L2\_05KMAPRO-STANDARD-V4-20, 2018.
- NASA/LARC/SD/ASDC: CALIPSO Lidar Level 3 Tropospheric Aerosol Profiles, All Sky Data, Standard V4-20, NASA Langley Atmospheric Science Data Center DAAC [data set], https://doi.org/10.5067/CALIOP/CALIPSO/CAL\_LID\_L3\_Tropospheric\_APro\_AllSky-Standard-V4-20, 2019.
- NASA Earth Data: AERDB\_M3\_VIIRS\_SNPP IRS/SNPP Blue Deep Level 3 monthly aerosol data,  $1 \times 1$ degree grid, NASA [data set], https://doi.org/10.5067/VIIRS/AERDB\_M3\_VIIRS\_SNPP.011, 2025.
- Quinn, P. K., Shaw, G., Andrews, E., Dutton, E. G., Ruoho-Airola, T., and Gong, S. L.: Arctic haze: current trends and knowledge gaps, Tellus B, 59, 99, https://doi.org/10.1111/j.1600-0889.2006.00236.x, 2007.
- Quinn, P. K., Bates, T. S., Baum, E., Doubleday, N., Fiore, A. M., Flanner, M., Fridlind, A., Garrett, T. J., Koch, D., Menon, S., Shindell, D., Stohl, A., and Warren, S. G.: Shortlived pollutants in the Arctic: their climate impact and possible mitigation strategies, Atmos. Chem. Phys., 8, 1723–1735, https://doi.org/10.5194/acp-8-1723-2008, 2008.
- Rahn, K. A., Borys, R. D., and Shaw, G. E.: The Asian source of Arctic haze bands, Nature, 268, 713–715, https://doi.org/10.1038/268713a0, 1977.
- Randles, C. A., Da Silva, A. M., Buchard, V., Colarco, P. R., Darmenov, A., Govindaraju, R., Smirnov, A., Holben, B., Ferrare, R., Hair, J., Shinozuka, Y., and Flynn, C. J.: The MERRA-2 Aerosol Reanalysis, 1980 Onward. Part I: System Description and Data Assimilation Evaluation, J. Climate, 30, 6823–6850, https://doi.org/10.1175/JCLI-D-16-0609.1, 2017.
- Remer, L. A., Levy, R. C., Mattoo, S., Tanré, D., Gupta, P., Shi, Y., Sawyer, V., Munchak, L. A., Zhou, Y., Kim, M., Ichoku, C., Patadia, F., Li, R.-R., Gassó, S., Kleidman, R. G., and Holben, B. N.: The Dark Target Algorithm for Observing the Global Aerosol System: Past, Present, and Future, Remote Sensing, 12, 2900, https://doi.org/10.3390/rs12182900, 2020.
- Sayer, A. M., Hsu, N. C., Bettenhausen, C., Ahmad, Z., Holben, B. N., Smirnov, A., Thomas, G. E., and Zhang, J.: SeaWiFS Ocean Aerosol Retrieval (SOAR): Algorithm, validation, and comparison with other data sets, J. Geophys. Res., 117, 2011JD016599, https://doi.org/10.1029/2011JD016599, 2012a.

- Sayer, A. M., Hsu, N. C., Bettenhausen, C., Jeong, M.-J., Holben, B. N., and Zhang, J.: Global and regional evaluation of over-land spectral aerosol optical depth retrievals from SeaWiFS, Atmos. Meas. Tech., 5, 1761–1778, https://doi.org/10.5194/amt-5-1761-2012, 2012b.
- Sayer, A. M., Munchak, L. A., Hsu, N. C., Levy, R. C., Bettenhausen, C., and Jeong, M.-J.: MODIS Collection 6 aerosol products: Comparison between Aqua's e-Deep Blue, Dark Target, and "merged" data sets, and usage recommendations, J. Geophys. Res.-Atmos., 119, https://doi.org/10.1002/2014JD022453, 2014.
- Sayer, A. M., Hsu, N. C., Lee, J., Carletta, N., Chen, S.-H., and Smirnov, A.: Evaluation of NASA Deep Blue/SOAR aerosol retrieval algorithms applied to AVHRR measurements, J. Geophys. Res.-Atmos., 122, 9945–9967, https://doi.org/10.1002/2017JD026934, 2017.
- Schmale, J., Zieger, P., and Ekman, A. M. L.: Aerosols in current and future Arctic climate, Nat. Clim. Chang., 11, 95–105, https://doi.org/10.1038/s41558-020-00969-5, 2021.
- Schmale, J., Sharma, S., Decesari, S., Pernov, J., Massling, A., Hansson, H.-C., von Salzen, K., Skov, H., Andrews, E., Quinn, P. K., Upchurch, L. M., Eleftheriadis, K., Traversi, R., Gilardoni, S., Mazzola, M., Laing, J., and Hopke, P.: Pan-Arctic seasonal cycles and long-term trends of aerosol properties from 10 observatories, Atmos. Chem. Phys., 22, 3067–3096, https://doi.org/10.5194/acp-22-3067-2022, 2022.
- Schmeisser, L., Backman, J., Ogren, J. A., Andrews, E., Asmi, E., Starkweather, S., Uttal, T., Fiebig, M., Sharma, S., Eleftheriadis, K., Vratolis, S., Bergin, M., Tunved, P., and Jefferson, A.: Seasonality of aerosol optical properties in the Arctic, Atmos. Chem. Phys., 18, 11599–11622, https://doi.org/10.5194/acp-18-11599-2018, 2018.
- Schueler, C. F., Lee, T. F., and Miller, S. D.: VIIRS constant spatial-resolution advantages, International Journal of Remote Sensing, 34, 5761–5777, https://doi.org/10.1080/01431161.2013.796102, 2013.
- Shaw, G. E.: The Arctic Haze Phenomenon, Bulletin of the American Meteorological Society, 76, 2403–2413, 1995.
- Shen, Z., Ming, Y., Horowitz, L. W., Ramaswamy, V., and Lin, M.: On the Seasonality of Arctic Black Carbon, J. Climate, 30, 4429–4441, https://doi.org/10.1175/JCLI-D-16-0580.1, 2017.
- Smith, S. E., Ting, M., Wu, Y., and Zheng, C.: Beyond the lock-downs: satellite observations of aerosol optical depth through 2020, the first year of the COVID-19 pandemic, Environ. Res. Lett., 17, 074036, https://doi.org/10.1088/1748-9326/ac7889, 2022.

- Tao, M., Wang, L., Chen, L., Wang, Z., and Tao, J.: Reversal of Aerosol Properties in Eastern China with Rapid Decline of Anthropogenic Emissions, Remote Sensing, 12, 523, https://doi.org/10.3390/rs12030523, 2020.
- Toth, T. D., Campbell, J. R., Reid, J. S., Tackett, J. L., Vaughan, M. A., Zhang, J., and Marquis, J. W.: Minimum aerosol layer detection sensitivities and their subsequent impacts on aerosol optical thickness retrievals in CALIPSO level 2 data products, Atmos. Meas. Tech., 11, 499–514, https://doi.org/10.5194/amt-11-499-2018, 2018.
- Vermote and A. Vermeulen: ATMOSPHERIC CORRECTION ALGORITHM: SPECTRAL REFLECTANCES (MOD09), https://modis.gsfc.nasa.gov/data/atbd/atbd\_mod08.pdf (last access: 12 November 2024), 1999.
- Virtanen, T. H., Kolmonen, P., Sogacheva, L., Rodríguez, E., Saponaro, G., and de Leeuw, G.: Collocation mismatch uncertainties in satellite aerosol retrieval validation, Atmos. Meas. Tech., 11, 925–938, https://doi.org/10.5194/amt-11-925-2018, 2018
- Wei, J., Li, Z., Peng, Y., and Sun, L.: MODIS Collection 6.1 aerosol optical depth products over land and ocean: validation and comparison, Atmospheric Environment, 201, 428–440, https://doi.org/10.1016/j.atmosenv.2018.12.004, 2019.
- Winker, D. M., Vaughan, M. A., Omar, A., Hu, Y., Powell, K. A., Liu, Z., Hunt, W. H., and Young, S. A.: Overview of the CALIPSO Mission and CALIOP Data Processing Algorithms, Journal of Atmospheric and Oceanic Technology, 26, 2310–2323, https://doi.org/10.1175/2009JTECHA1281.1, 2009.
- Wolfe, R. E., Lin, G., Nishihama, M., Tewari, K. P., Tilton, J. C., and Isaacman, A. R.: Suomi NPP VIIRS prelaunch and on-orbit geometric calibration and characterization, J. Geophys. Res.-Atmos., 118, https://doi.org/10.1002/jgrd.50873, 2013.
- Yang, Y., Lou, S., Wang, H., Wang, P., and Liao, H.: Trends and source apportionment of aerosols in Europe during 1980–2018, Atmos. Chem. Phys., 20, 2579–2590, https://doi.org/10.5194/acp-20-2579-2020, 2020.
- Zhao, C. and Garrett, T. J.: Effects of Arctic haze on surface cloud radiative forcing, Geophysical Research Letters, 42, 557–564, https://doi.org/10.1002/2014GL062015, 2015.